JPn Neuroscience

The Journal of Physiology

J Physiol 590.16 (2012) pp 3719–3741

Properties of subependymal cerebrospinal fluid contacting neurones in the dorsal vagal complex of the mouse brainstem

Adeline Orts-Del'Immagine, Nicolas Wanaverbecq, Catherine Tardivel, Vanessa Tillement, Michel Dallaporta and Jérôme Trouslard

Laboratoire de Physiologie et Physiopathologie du Système Nerveux Somato-moteur et Neurovégétatif (PPSN) EA 4674 Aix-Marseille Université (AMU), Faculté des Sciences et Techniques St. Jérôme, BP 352, Avenue Escadrille Normandie Niemen, F-13397 Marseille cedex 20, France

Key points

- The brainstem is a major site of integration for autonomic information from neurones, blood and cerebrospinal fluid (CSF). Signals exchange from the CSF is limited by the ependymocytes forming the brain cavities. However neurones contacting the CSF (CSF-cNs) are thought to integrate those signals.
- Using immunohistochemical and electrophysiological approaches, we characterise in the brainstem, subependymal CSF-cNs projecting a process ending in the central canal with a protrusion and expressing a 'transient receptor potential' (TRP) channel subtype suggested to act as chemo- or mechanoreceptors: the polycystin kidney disease 2-like 1 channels (PKD2L1).
- CSF-cNs receive exclusively inhibitory synaptic inputs and express functional channels presenting all properties of PKD2L1: cationic non-selective, large conductance and modulated by extracellular pH and osmolarity.
- Because medullar CSF-cNs are strategically positioned between CSF and neuronal parenchyma, we hypothesise that they could play a role in the regulation of homeostasis by integrating CSF signals.

Abstract Cerebrospinal fluid (CSF) contacting neurones have been observed in various brain regions such as the hypothalamus, the dorsal nucleus of the raphe and around the central canal (cc) of the spinal cord but their functional role remains unclear. At the level of the spinal cord, subependymal cerebrospinal fluid contacting neurones (S-CSF-cNs) present a peculiar morphology with a soma close to the ependymal layer, a process projecting towards the cc and ending with a bud and a cilium. These neurones were recently shown to express polycystin kidney disease 2-like 1 (PKD2L1 or TRPP3) channels that are members of the polycystin subtype of the transient receptor potential (TRP) channel superfamily and that have been proposed as either chemo- or mechanoreceptors in several tissues. Using immunohistological techniques and whole-cell electrophysiological recordings in brain slices obtained from PKD2L1:EGFP transgenic adult mice, we looked for and determined the functional properties of S-CSF-cNs in the dorsal vagal complex (DVC), a hindbrain structure controlling autonomic functions such as blood pressure, energy balance and food intake. Here, we demonstrate that S-CSF-cNs received GABAergic and/or glycinergic synaptic entries and were also characterised by the presence of non-selective cationic channels of large conductance that could be detected even under whole-cell configuration. The channel activity was not affected by *Psalmopoeus cambridgei* toxin 1, a blocker of acid sensing ion channels (ASICs), but was blocked by amiloride and by a strong extracellular acidification. In contrast, extracellular alkalinisation and hypo-osmotic shocks increased channel activity. Based on these properties, we suggest that the single-channel activity recorded in medullar S-CSF-cNs is carried by PKD2L1 channels. Our study therefore reinforces the idea that PKD2L1 is a marker

A. Orts-Del'Immagine and N. Wanaverbecq contributed equally to the work.

DOI: 10.1113/jphysiol.2012.227959

of S-CSF-cNs and points toward a role for S-CSF-cNs in the detection of circulating signals and of modifications in the extracellular environment.

(Received 30 January 2012; accepted after revision 2 May 2012; first published online 8 May 2012)

Corresponding author J. Trouslard: Laboratoire de Physiologie et Physiopathologie du Système Nerveux Somato-moteur et Neurovégétatif (PPSN) EA 4674 Aix-Marseille Université (AMU), Faculté des Sciences et Techniques St. Jérôme, BP 352, Avenue Escadrille Normandie Niemen, F-13397 Marseille cedex 20, France. Email: jerome.trouslard@univ-amu.fr

Abbreviations AP, action potential; ASIC, acid sensing ion channel; CSF, cerebrospinal fluid; S-CSF-cN, subependymal cerebrospinal fluid contacting neurone; cc, central canal; DVC, dorsal vagal complex; EGFP, enhanced green fluorescence protein; LED, light-emitting diode; 2-Me-S-ATP, 2-methylthioadenosine triphosphate; PFA, paraformaldehyde; PcTx1, psalmotoxin 1 or *Psalmopoeus cambridgei* toxin 1; PKD2L1, polycystin kidney disease 2-like 1; TRPP, transient receptor potential/polycystin.

Introduction

In the central nervous system (CNS) of vertebrates, neurones in contact (CSF-cNs) with the cerebrospinal fluid (CSF) had already been described in the late 19th century and were suggested to be part of the circumventricular organs and potentially involved in information transfer from and to the CSF (Vigh & Vigh-Teichmann, 1998; Vígh *et al.* 2004). In mammals, this neuronal population is sparsely distributed in several brain regions with exact projection pathways and physiological function largely unknown (Sancesario *et al.* 1996; Zhang *et al.* 2003; Xiao *et al.* 2005). CSF-cNs have been identified in hypothalamic nuclei where they might take part in neuroendocrine regulations (Vígh & Vígh-Teichmann, 1998; Xiao *et al.* 2005). They have also been observed in the dorsal raphe nucleus, a brain region involved in pain modulation and anti-nociception function (Wang & Nakai, 1994; Chuma *et al.* 2002). The largest number of CSF-cNs is found in the region surrounding the central canal (cc) of the spinal cord, a plastic zone capable of limited endogenous repairs in the event of spinal injuries (Mothe & Tator, 2005; Meletis *et al.* 2008). Recent studies have suggested that spinal CSF-cNs might be important elements of the spinal neurogenic niche because they are present at different stages of neuronal maturity and express molecules involved in migration and differentiation of immature neurones (Stoeckel *et al.* 2003; Marichal *et al.* 2009).

Huang and colleagues (2006) recently developed a transgenic mouse model where EGFP is selectively expressed in polycystin kidney disease 2-like 1 (PKD2L1) positive cells. In the same study, these authors demonstrated the presence of PKD2L1 in spinal CSF-cNs. They also suggested, without analysing their properties, that CSF-cNs are present in the brainstem and the hypothalamus, two major cerebral structures involved in the control of autonomic functions. PKD2L1 (Polycystin-L or TRPP3 channels, HUGO nomenclature) are members of the polycystin subgroup of the 'transient receptor potential' (TRP) superfamily and their activity was shown to be modulated by variation in extracellular pH (Inada *et al.* 2008; Shimizu *et al.* 2009; Kawaguchi *et al.* 2010) and osmolarity (Murakami *et al.* 2005; Shimizu *et al.* 2009). Polycystin channels are present in various tissues – including kidney, retina and testis but also brain tissues (Wu *et al.* 1998; Basora *et al.* 2002). Although the exact functions of polycystin channels remain unclear in the brain, they are often associated with sensory integration of extracellular signals such as mechanodetection (Nauli *et al.* 2003) and chemoreception (Ishimaru *et al.* 2006; Huang *et al.* 2006; Ishii *et al.* 2009; Kawaguchi *et al.* 2010) in other tissues. Therefore, and because they are strategically positioned between CSF and parenchyma, PKD2L1 expressing CSF-cNs, could have functions in chemo- and/or mechanodetection of CSF signals and take part in the control of CSF homeostasis. They could also detect information from the CSF and convey the collected messages to cellular partners. Such a role for CSF-cNs might be particularly relevant at the level of the brainstem since this structure represents a major regulatory site for autonomic functions and integrates neuronal, humoral and CSF circulating signals (Guyenet, 2006; Schwartz, 2006). However, the presence of CSF-cNs in the brainstem has only been suggested and nothing is known about their electrophysiological properties.

By combining immunohistological and patch-clamp electrophysiological approaches in adult EGFP:PKD2L1 transgenic mice, we demonstrate that PKD2L1$^+$ cells are indeed present around the cc in the dorsal vagal complex (DVC) of the brainstem. These subependymal CSF-cNs (S-CSF-cNs) have a similar morphology to that observed for spinal S-CSF-cNs and mostly receive inhibitory synaptic inputs. We further demonstrate that medullar S-CSF-cNs exhibit a spontaneous single-channel activity sharing all properties known for PKD2L1 channels. The present study corresponds to the first characterisation of S-CSF-cNs in the brainstem and represents a further step in understanding the physiological role of this peculiar neuronal population.

Methods

Ethical approval

All experiments were conducted in conformity with the rules set by the EC Council Directive (2010/63/UE) and the French 'Direction Départementale de la Protection des Populations des Bouches-du-Rhône' (Licence no. 13.435 held by J.T. and no. 13.430 by N.W.). Protocols used are in agreement with the rules set by the Comité d'Ethique de Marseille, our local Committee for Animal Care and Research. Every precaution was taken to minimise animal stress and the number of animals used.

General

We used 8- to 10-weeks-old PKD2L1:EGFP transgenic mice (*Mus musculus*) obtained by crossing PKD2L1-IRES-Cre with Z/EG (lacZ/EGFP) reporter transgenic mice. Thus, in PKD2L1$^+$ cells, EGFP expression is selectively induced by Cre recombinase activity (Huang *et al.* 2006). PKD2L1-IRES-Cre mice were a generous gift from Dr C. S. Zuker (Howard Hughes Medical Institute, University of California, La Jolla, CA, USA) and Z/EG reporter lines were kindly provided by Dr P. Durbec (IBDML, Université de la Méditerranée, Marseille, France). All animals were housed at constant temperature (21°C) under a standard 12 h light−12 h dark cycle, with food (pellet AO4, UAR, Villemoisson-sur-Orge, France) and water provided *ad libitum*. Data were obtained from 104 transgenic PKD2L1:EGFP adult mice.

Animal genotyping

To assess EGFP expression in PKD2L1$^+$ cells, we carried out PCR on tail genomic DNA from 4- to 5-weeks-old male and female mice. CRE transgene was detected using the forward primer 5′-CGT ACT GAC GGT GGG AGA AT-3′ and the reverse primer 5′-CCC GGC AAA ACA GGT AGT TA-3′, with the following PCR conditions: 7 min at 95°C, 35 cycles at 95°C for 40 s, 62°C for 40 s and 72°C for 40 s, followed by a final step at 72°C for 6 min. The amplicon size was 166 bp. EGFP was detected using the forward primer 5′-GCC ACA AGT TCA GCG TGT CC-3' and the reverse primer 5′-GCT TCT CGT TGG GGT CTT TGC-3′, with the following PCR conditions: 5 min at 95°C, 36 cycles at 95°C for 30 s, 62°C for 30 s and 72°C for 40 s, followed by a final step at 72°C for 7 min. The amplicon size was 573 bp.

Slice preparation and electrophysiology

Brainstem slice preparation. Adult mice (8–10 weeks old) were anaesthetised with an intraperitoneal injection of ketamine (Carros, France) and xylazine (Puteau, France) mixture (100 and 15 mg kg^{-1}, respectively). Coronal brainstem slices were prepared as previously described by Roux *et al.* (2009). Briefly, anaesthetized animals were decapitated, and the brain rapidly removed and submerged in ice-cold (0–4°C), oxygenated (95% O_2 and 5% CO_2) low calcium/high magnesium artificial cerebrospinal fluid (aCSF) containing (in mM): NaCl 130, $NaHCO_3$ 26, NaH_2PO_4 1.25, KCl 3, $CaCl_2$ 0.5, $MgCl_2$ 7, glucose 15, ascorbic acid 0.5, sodium pyruvate 2, *myo*-inositol 3 (pH 7.3–7.4, osmolality ∼310 mosmol kg^{-1}). Coronal brainstem slices (200 μm thick) were cut with a vibrating blade microtome (Leica VT1000S) and transferred in a submerged recovery chamber filled with standard oxygenated aCSF maintained at 35°C containing (in mM): NaCl 130, $NaHCO_3$ 26, NaH_2PO_4 1.25, KCl 3, $CaCl_2$ 2, $MgCl_2$ 2, glucose 15, ascorbic acid 0.5, sodium pyruvate 2, *myo*-inositol 3 (pH 7.3–7.4, osmolality ∼310 mosmol kg^{-1}). Slices were allowed to return from 35°C to room temperature for 1 h and subsequently kept under continuous oxygenation until their transfer one by one to the recording chamber.

Electrophysiological recordings. At the beginning of each experiment, a slice was transferred to the recording chamber mounted on an upright microscope (Zeiss Axioskop 1FS) equipped with infra-red differential interference contrast imaging (IR-DIC) and a p1 precisExcite LED epifluorescence system (CooLED, Roper). PKD2L1:EGFP$^+$ cells and AlexaFluor 594 fluorescence were visualised under 490 nm and 590 nm illumination, respectively, and images captured with a CoolSNAP HQ^2 cooled CCD camera (Photometrics) connected to a computer through a frame grabber (CoolSNAP LVDS interface card, Photometrics) controlled by MetaView software (Molecular Devices Inc., Sunnyvale, CA, USA) (Figs 1*A*–*C* and 2*A*). Recordings were restricted to cells located around the cc that exhibited a process extending toward the cc, ending with a bud, and identified as subependymal CSF-cNs (S-CSF-cNs; see in Fig. 1*B* inset, open triangles, and Fig. 1*C*). Typically, in a slice, an EGFP$^+$ cell with the characteristic morphological properties of S-CSF-cNs was spotted under 490 nm illumination. The whole-cell configuration was obtained under IR-DIC illumination with a patch pipette containing 10 μM AlexaFluor 594 (Invitrogen) to confirm that the recorded cell was the selected one (Fig. 2*A*). This procedure also allowed us, on some occasions, to record S-CSF-cNs even using brain slices obtained from EGFP negative animals. Whole-cell patch-clamp recordings were performed in current- and/or voltage-clamp mode using a Multiclamp 700B patch-clamp amplifier (Molecular Devices). Patch pipettes were pulled from borosilicate glass capillaries (Harvard Apparatus, Les Ulis, France) and filled using an internal solution with composition detailed in Table 1.

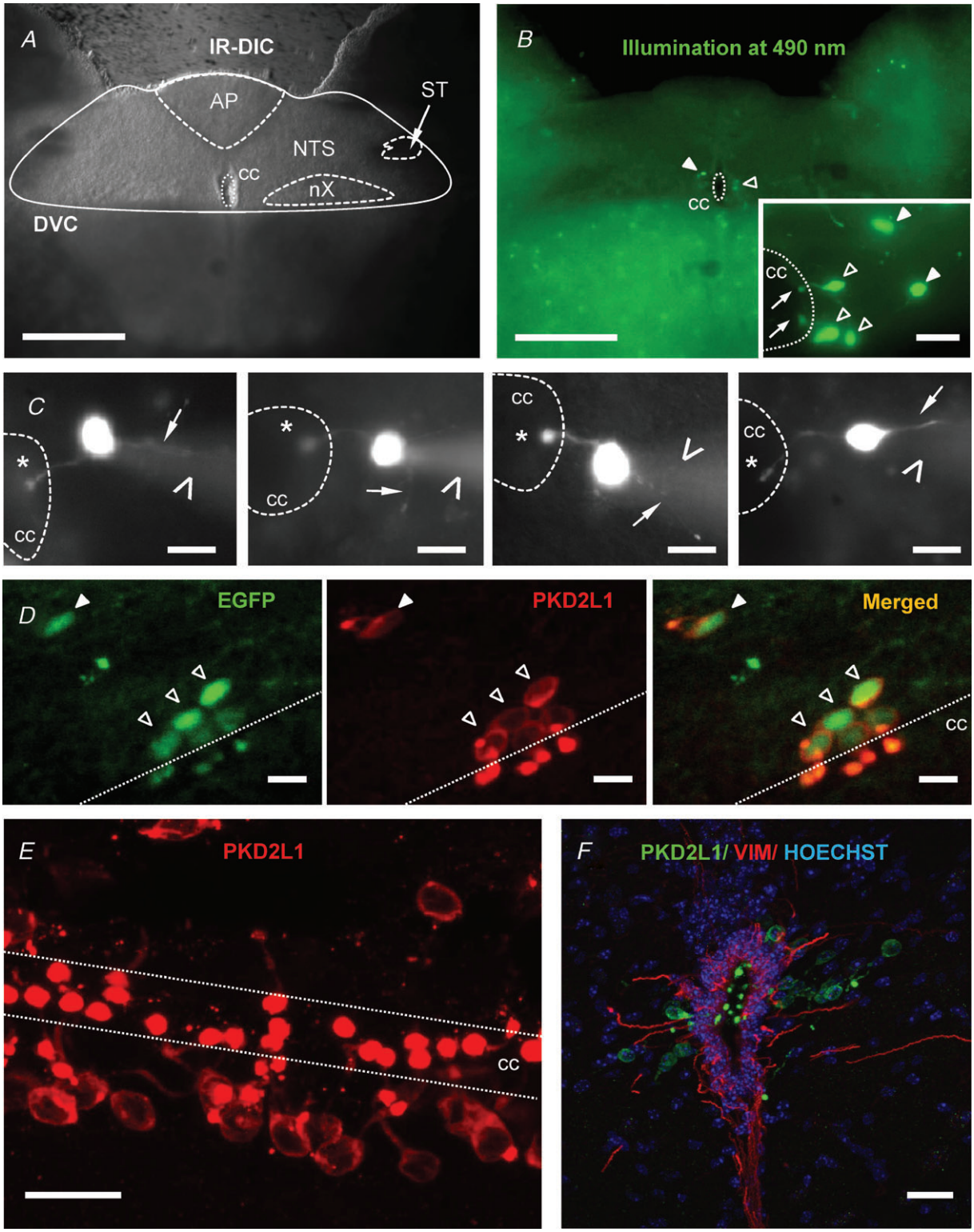

Figure 1. In the dorsal vagal complex S-CSF-cNs are present and express PKD2L1 channels
A, acute coronal brainstem slice observed under infrared differential interference contrast (IR-DIC) illumination showing the characteristic structures of the dorsal vagal complex (DVC). AP, area postrema; NTS, nucleus tractus solitarii; ST, solitary tract; nX, dorsal motor nucleus of the vagus nerve; cc, central canal. *B*, in the same acute brainstem slice as in *A*, under 490 nm illumination, $EGFP^{+}$ cells were observed close to the cc and in the parenchyma. Inset shows at higher magnification that $EGFP^{+}$ cells close to the cc project a single process ending with a protrusion in the cavity (arrow) while cells in the parenchyma do not. *C*, selected representative micrographs

The tip resistance of the electrodes was 5–7 MΩ when filled with the intracellular solution. Access resistances, in the whole-cell configuration, ranged between 10 and 20 MΩ and were not compensated. The access resistance (r_S) was monitored with a −20 mV calibration pulse regularly applied throughout each experiment. Recording was stopped when r_S exceeded by more than 25% the original value. Typically, signals were filtered at 2.4 kHz, digitised between 10 and 20 kHz, and then acquired on a computer using the pCLAMP 9.2 suite (Molecular Devices).

Slice perfusion and drug application. Slices were continuously superfused at a rate of 2.5 ml min^{-1} with oxygenated standard aCSF (see composition above) maintained at room temperature (∼20°C). Unless otherwise stated, all chemicals and drugs were purchased from Sigma-Aldrich. Selective antagonists or blockers were bath applied to block receptors and channels as follows: ionotropic glutamatergic receptors with 1 mM kynurenic acid; $GABA_A$ receptors with 10 μM gabazine (SR 95531, Ascent Scientific, Bristol, UK); glycine receptors with 1–10 μM strychnine; TRP and ASIC channels with amiloride 2 mM; and ASIC channels with 40 nM *Psalmopoeus cambridgei* toxin 1 (psalmotoxin 1 or PcTX1, a gift from Drs S. Diochot and E. Lingueglia). GABA, glycine, ATP, 2-methylthioadenosine triphosphate tetrasodium salt (2-Me-S-ATP, Tocris) and amiloride (Fig. 6*C*) were applied using a patch-clamp pipette connected to a pressure application system (Toohey Company) to allow rapid and focal application as well as rapid wash. Experiments were also performed using pressure application of aCSF in the absence of drugs in order to test for the existence of application artefacts or mechanical responses. However, no change in the holding current was observed in any of those control experiments confirming that effects were drug or test solution specific.

To force vesicular release and allow the characterisation of low frequency synaptic events, a hyperosmotic shock was used by adding 500 mM sucrose to the standard aCSF solution (final osmolality of 800 mosmol kg^{-1}). This solution was pressure applied for 10–30 s onto the recorded cells (see Fig. 3*B*–*E*).

Modulation of single-channel activity by variations in extracellular pH was determined using pressure application of test solutions at various pH values. Alkaline solution at pH 8.8 had the following composition (mM): NaCl 145, KCl 3, $CaCl_2$ 2, $MgCl_2$ 2, glucose 15, Hepes 10, (*N*-tris(hydroxymethyl)methyl-3-aminopropanesulfonic acid (TAPS) 10 (pH 8.8 adjusted with NaOH 1 M; ∼310 mosmol kg^{-1}). The HCl pH 2.8 solution was prepared using (mM): NaCl 145, KCl 3, $CaCl_2$ 2, $MgCl_2$ 2, glucose 15, sucrose 10, Hepes 10 (pH 2.8 adjusted with HCl 1 M; ∼310 mosmol kg^{-1}). To prepare the citric acid-based acidic solutions we added to the standard aCSF the citric acid/sodium citrate couple (final concentration 30 mM) in proportions enabling final pH values of 6.3, 6.0, 5.5, 5.0 and 2.8 (∼310 mosmol kg^{-1}). To assess the osmosensitivity of channel activity, we used a modified control aCSF of the following composition (mM): NaCl 115, $NaHCO_3$ 26, NaH_2PO_4 1.25, KCl 3, $CaCl_2$ 2, $MgCl_2$ 2, sucrose 45, ascorbic acid 0.5, sodium pyruvate 2, *myo*-inositol 3 (pH 7.3–7.4, and osmolality of ∼310 mosmol kg^{-1}). For the hypo-osmotic solution 45 mM sucrose was removed from the solution (osmolality of ∼265 mosmol kg^{-1}) while for the hyper-osmotic solution the sucrose concentration was increased to 90 mM (osmolality of ∼355 mosmol kg^{-1}) without modifying the ionic concentration. These solutions were pressure applied for 3 min. The osmolality of all solutions was measured using a calibrated micro-osmometer (Roebling MessTechnick).

Analysis and statistics. Passive properties were determined, in voltage-clamp mode at −80 mV, from the cell current responses to a −20 mV hyperpolarisation step (V_{step}). Membrane resistance (r_m) was calculated from the amplitude of the sustained current at the end of the voltage step ($r_m = V_{step}/I_m$). Membrane capacitance (c_m) was estimated as the ratio between the cell decay time constant (τ), obtained from the exponential fit of the current decay, divided by r_S ($c_m \sim \tau/r_S$). Resting membrane potential was determined

illustrating 4 different neurones recorded in the whole-cell configuration with an intracellular solution containing 10 μM AlexaFluor 594 to reveal the cellular morphology. Star: round protrusion or bud in the CSF cavity; thin arrow: thin neurite resembling the axon; arrow head: shadow of the patch pipette. Note that images are presented in greyscale for a better visualisation. *D*, sagittal brainstem section showing that EGFP$^+$ cells (left) in contact with the cc or in the parenchyma exhibit PKD2L1 positive immunoreactivity (middle). Right, merged image showing that all EGFP$^+$ cells were also PKD2L1$^+$. *E*, sagittal section showing the high density of PKD2L1$^+$ cells along the cc of the brainstem. *F*, brainstem coronal section showing PKD2L1$^+$ cells (green) inserted between vimentin positive ependymal cells (VIM, red). Nuclei were visualised using Hoechst coloration (blue). In *A*–*E*, thin dashed line delineates cc. Open triangles: cells in contact with cc; filled triangles: cells in the parenchyma. Scale bars: *A* and *B*, 100 μm; inset in *B* and *D*–*F*, 20 μm and *C*, 10 μm. Objective: 5× in *A* and *B*; 63×, *B* inset, *C*–*E*; 20x in *F*. *A*–*C*: epifluorescence imaging; *D*–*F*: confocal Z projections.

in current-clamp mode at $I = 0$ just after the whole-cell configuration was achieved. Current responses to agonists were analysed using the Clampfit 9.2 suite (Molecular Devices) and Microsoft Excel 2007. Spontaneous synaptic current amplitude, rise time, frequency and decay time constant were determined using either the 'template event detection' routine from the Clampfit 9.2 suite (Molecular Devices) or Mini Analysis Software (Synaptosoft, Inc., Decatur, GA, USA). Single-channel activity was analysed over 10–60 s periods selected in each condition with the 'single-channel detection' routine from the Clampfit 9.2 suite to determine unitary current amplitude and opening durations. Typically, the channel opening probability (NP_O with N the number of channels and P_O the channel open probability) was calculated as the sum of open times divided by the time of analysis in each condition. We also carried out single channel analysis by determining the probability density function (PDF) using amplitude distribution histograms. Unitary current amplitude was measured as the peak-to-peak distance in Gaussian fits. Both analytic approaches gave equivalent results in the measure of single channel properties.

In each set of experiments, normalisation was calculated as the ratio between experimental data points obtained in a given condition (control, test or wash) divided by the average control value for the pooled data. All averaged data presented are given as means ± SEM. Statistical significance, assuming a non-Gaussian distribution, was determined using Kruskal–Wallis, non-parametric Mann–Whitney or Wilcoxon's matched-pairs signed rank statistical tests. Differences were considered statistically significant for $P < 0.05$. Statistical analysis was carried out with Prism 5.0.4 (GraphPad Software Inc., La Jolla, CA, USA).

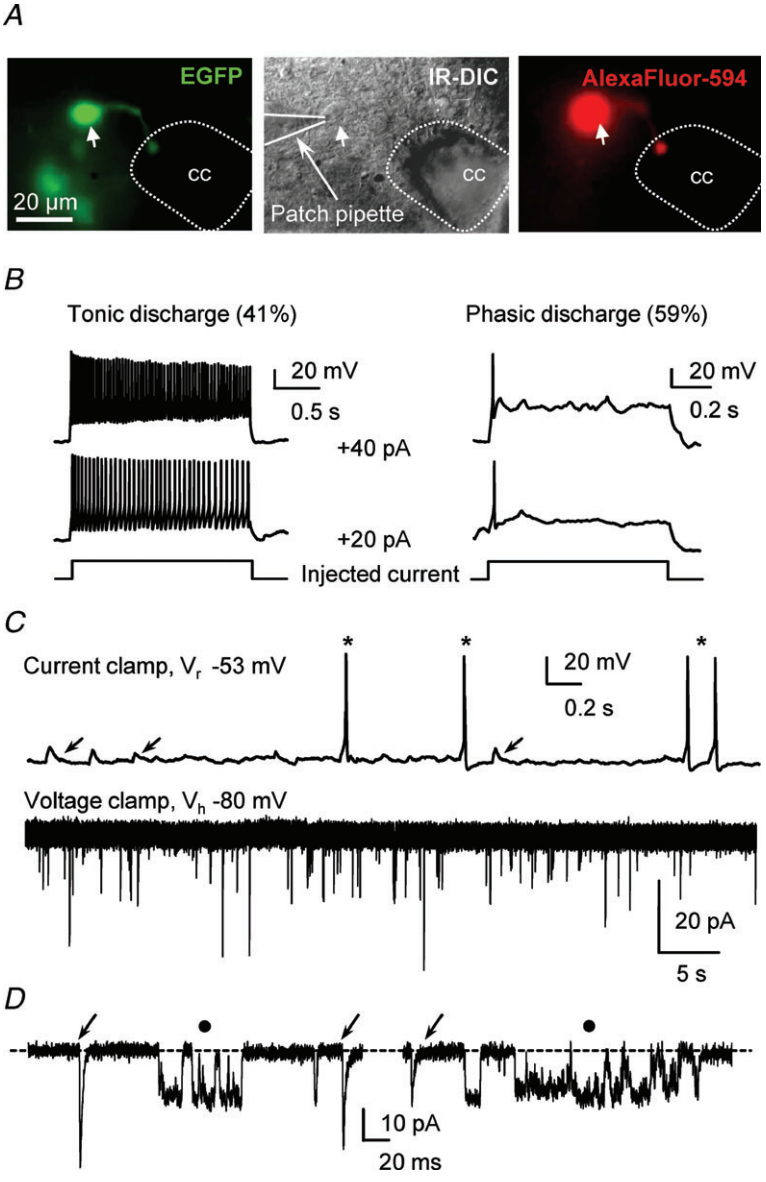

Figure 2. PKD2L1:EGFP$^+$ cells are neurones and exhibit both synaptic and unitary single-channel activities
A, one PKD2L1:EGFP$^+$ subependymal CSF-cN (Left) was patched under IR-DIC illumination (middle) with a pipette solution containing 10 μM AlexaFluor 594. After cell dialysis, AlexaFluor 594 fluorescence confirmed that the identified PKD2L1:EGFP$^+$ neurone was recorded (right). Arrow points to the neuronal somata. *B*, two representative S-CSF-cNs recorded in current-clamp mode at −60 mV (current injected to maintain the membrane potential at −60 mV: −12 pA left panel; −18 pA right panel) exhibiting either tonic (left panel) or phasic (right panel) action potential (AP) discharge in response to depolarising current injection (+20 pA, +40 pA). Note that while the tonic neurone responded with a higher AP discharge frequency when the injected current increased from +20 to +40 pA, the phasic neurone still generated a single AP. *C*, top, current-clamp trace from a S-CSF-cN recorded at resting potential ($V_r = -53$ mV) showing spontaneous depolarising events (arrows) as well as spontaneous AP discharge (star). Bottom, at −80 mV (V_h) in voltage-clamp mode, the same neurone exhibited spontaneous inward currents. *D*, expanded portions, selected from the recording in *C*, showing that S-CSF-cNs exhibited both fast inward currents resembling synaptic events (arrows) and currents with a square time course (filled circle) characteristic of single-channel activity. Dashed line indicates channel closed state.

Table 1. Composition of the intracellular recording solutions

Composition (mM)	KCl	K-gluconate	CsCl	Cs-acetate	
NaCl	10	10	10	4	10
KCl	135	20	—	—	—
CsCl	—	—	135	—	20
CsAc	—	—	—	135	120
K-gluconate	—	115	—	—	—
$MgCl_2$			2		
$CaCl_2$			1		
Free $[Ca^{2+}]_i$			13 nM		
EGTA			5		
Hepes			10		
Phosphocreatine			10		
Na_2-ATP			4		
Ionic reversal potentials (mV) at 20°C					
E_{Na}	+55	+55	+55	+65	+55
E_K	−96	−96	na	na	na
E_{Cl}	+2	−34	+2	−67	−34
pH			7.30 – 7.35		
Adjusted with	KOH 1 M	KOH 1 M	CsOH 50% v/v	CsOH 50% v/v	CsOH 50% v/v
Osmolality			set to ∼290 mosmol kg^{-1}		

Composition of the intracellular solutions used to characterise the electrophysiological properties of S-CSF-cNs with the mention of the ionic reversal potential for sodium (E_{Na}), potassium (E_K) and chloride (E_{Cl}) ions. Potassium chloride-based solution (KCl): experiments illustrated in Figs 2*B–D* and 3*A* for GABAergic currents; potassium gluconate-based solution (K-gluconate): experiments illustrated in Figs 3*A* for glycinergic currents, 5*A* and *B*, and 7; caesium chloride-based solution (CsCl): experiments illustrated in Figs 4*A–C*, 5*C* and *D*, 6 and 8; caesium acetate-based (CsAc) solution with E_{Cl} set at −34 mV: experiments illustrated in Fig. 3*B–E*; and caesium acetate-based (CsAc) solution with E_{Cl} set at −67 mV: experiments illustrated in Fig. 4*D*. All solutions were controlled for osmolality (∼290 mosmol kg^{-1}) and pH was adjusted to 7.30–7.35 as mentioned in the table.

Immunohistochemistry

Mice were anaesthetised with a ketamine–xylazine mixture (see above, Slice preparation and electrophysiology) and were transcardially perfused first with phosphate buffer solution (PBS; 0.1 M). Subsequently the animals were perfused with 4% paraformaldehyde (PFA) in 0.1 M PBS. Brains were immediately removed, post-fixed 1 h in PBS–4% PFA at 4°C, cryoprotected for 24–48 h in 30% sucrose at 4°C and frozen in isopentane (−40°C). Brainstem coronal and sagittal thin sections (40 μm) were obtained using a cryostat (Leika CM3050) and collected serially in 12-well plates containing 0.1 M PBS. Slices were incubated 1 h in PBS containing 0.3% Triton X-100 (Sigma) and 3% horse serum with 1% bovine serum albumin (BSA) for rabbit anti-PKD2L1 IgG (1:700) and 4% normal goat serum for chicken anti-vimentin IgG (1:2000). Slices were incubated overnight at 4°C with primary antibodies. Sections were then washed in PBS and incubated for 2 h with secondary antibodies conjugated to either AlexaFluor 488 or 594 (1:400). Primary and secondary antibodies were purchased from Millipore-Chemicon. Nuclear visualisation was achieved using bis-benzimide (Hoechst) coloration (1 μg ml^{-1} for 1–2 min, Sigma-Aldrich). Sections were mounted on gelatin coated slides and coverslipped with home-made mowiol mounting medium for fluorescence microscope preparation. Slides were observed and images acquired using a confocal microscope (Zeiss LSM700). Images were analysed and prepared using ZEN 2009 light Edition (Zeiss software) and ImageJ 1.45 (NIH).

Results

In the dorsal vagal complex, cells with S-CSF-cN morphology are present and express PKD2L1

When using their transgenic PKD2L1:EGFP$^+$ mice, Huang and colleagues (2006) suggested the presence of PKD2L1:EGFP$^+$ cells in the brainstem. As a preliminary step in our study and to confirm this assumption, we prepared coronal brainstem slices from transgenic PKD2L1:EGFP$^+$ mice and looked for EGFP$^+$ cells in this structure. Typically, we used slices at the postremal level containing the dorsal vagal complex (DVC) with its characteristic structures (Fig. 1*A*; Roux *et al.* 2009).

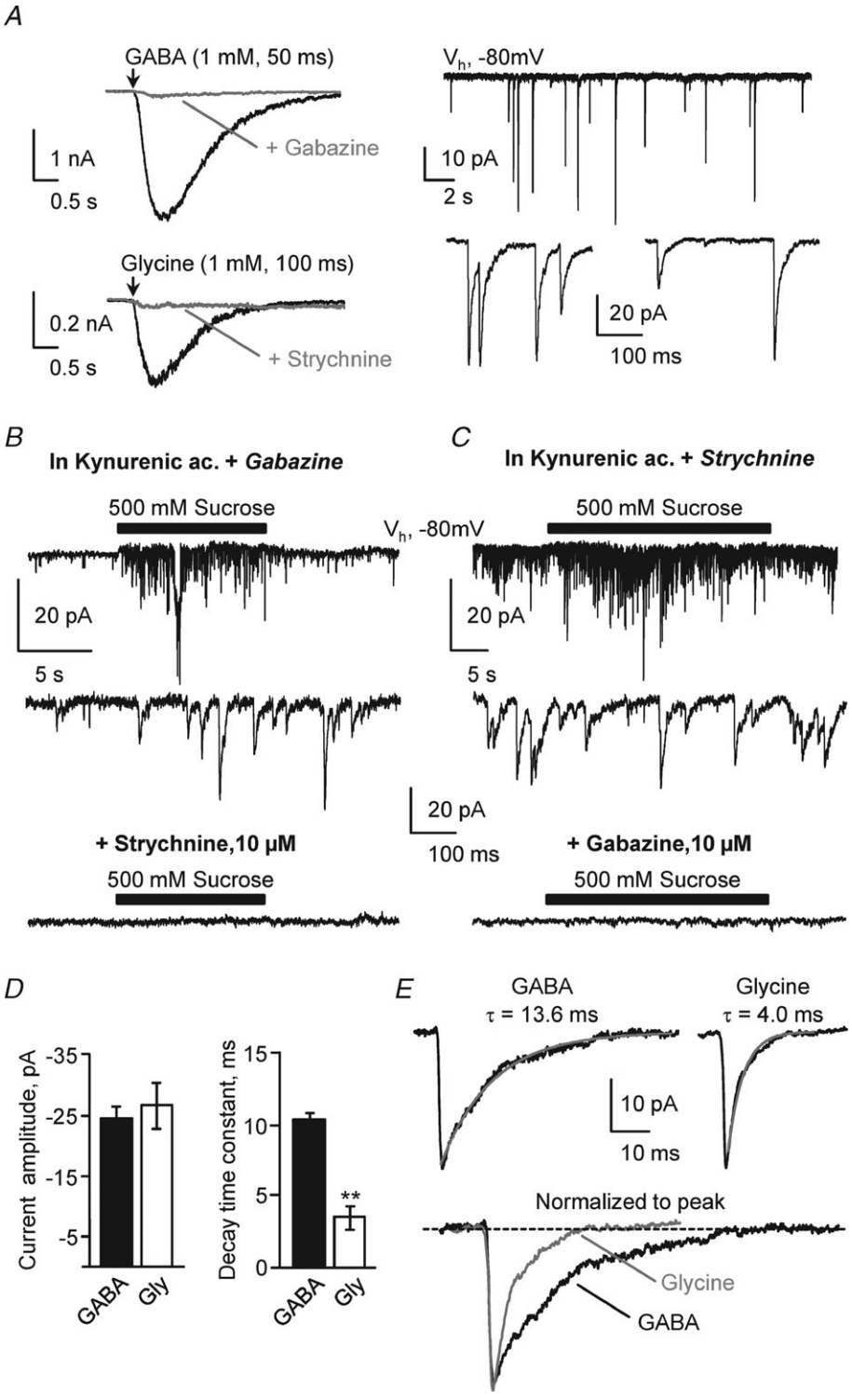

Figure 3. S-CSF-cNs possess functional synaptic $GABA_A$ and glycine receptors
A, left, representative current traces recorded at −80 mV in two S-CSF-cNs in response to pressure application of GABA (top; 1 mM, 50 ms, arrow) and glycine (bottom; 1 mM, 100 ms, arrow). In the presence of 10 μM gabazine (top) or 10 μM strychnine (bottom), pressure application of GABA or glycine, respectively, markedly reduced the elicited currents (grey traces). Right, spontaneous inward current activity recorded in voltage-clamp mode at −80 mV (V_h), in the presence of 1 mM kynurenic acid, a broad spectrum ionotropic glutamate receptors antagonist, to block fast glutamatergic transmission. Bottom, expanded portions selected from the current trace at the top showing that inward currents were of synaptic nature with a fast onset and an exponential decay. *B*, top, in the presence of 1 mM kynurenic acid and 10 μM gabazine, to block both glutamatergic and GABAergic transmission,

When acute DVC coronal slices, obtained from PKD2L1:EGFP$^+$ mice, were illuminated at 490 nm in the recording chamber, EGFP$^+$ cells (peak emission at 520 nm) were visualised around the central canal (cc; Fig. 1*B*). At this level, EGFP$^+$ cells had the characteristic morphology of spinal S-CSF-cNs (Stoeckel *et al.* 2003; Marichal *et al.* 2009) with small circular-shaped soma (diameter: 9.8 ± 0.3 μm; $n = 30$) from which a process projected towards the cavity and ended in the cc with a spherical protrusion or bud (diameter: 4.0 ± 0.1 μm; $n = 30$) (Figs 1*B* inset, 1*C*–*F* and 2*A*). Although at the spinal cord level, S-CSF-cNs were suggested to bear a cilia on the bud (Stoeckel *et al.* 2003; Marichal *et al.* 2009), we never visualised such a structure on medullar S-CSF-cNs. Following whole-cell patch-clamp recording and cell dialysis with an intracellular solution containing 10 μM AlexaFluor 594, a thin projection (thin arrows in Fig. 1*C*) resembling the axon could be visualised. Such thin processes could also be observed during visualisation of PFA-fixed brainstem coronal and horizontal sections obtained from EGFP$^+$ animals (data not shown). In some instances small enlargements resembling varicosities could be observed along these thin processes (data not shown), but a dedicated morphological study needs to be carried out to confirm their axonal nature. Note that in coronal DVC slices, these thin projections could only be followed over a very short distance suggesting, as proposed by Stoeckel *et al*. (2003), that S-CSF-cN axons might run in the longitudinal plane.

Using the PKD2L1:EGFP mice model, EGFP$^+$ cells should also express PKD2L1 proteins. To validate our experimental model and confirm the EGFP/PKD2L1 double expression, we carried out immunohistochemical experiments using a selective antibody against PKD2L1. As illustrated on Fig. 1*D*, EGFP$^+$ cells around the cc showed positive immunoreactivity for PKD2L1 protein on their soma, along the neurite and, with a higher intensity, on the bud, thus confirming that in sections of fixed tissue obtained from PKD2L1:EGFP$^+$ animals, all EGFP$^+$ cells also expressed PKD2L1. These cells were distributed along the axis of the cc, as can be visualised on a sagittal section in Fig. 1*E*, but the density of S-CSF-cNs, very high at the spinal level, progressively diminished towards more rostral part of the cc with only few PKD2L1$^+$ cells present next to the 4th ventricle (data not shown). PKD2L1:EGFP$^+$ cells were also present in the medullar parenchyma with no apparent contact with the cc (filled triangles in Fig. 1*B* and *D*). Finally, Fig. 1*F* shows that, around the cc, S-CSF-cNs were inserted between or close to ependymal cells labelled by an antibody raised against vimentin.

In the rest of our study, we focused our attention exclusively on S-CSF-cNs around the cc of the DVC and carried out their electrophysiological characterisation.

S-CSF-cN passive electrophysiological properties

As expected from their small size, S-CSF-cNs had a small mean membrane capacitance (3.4 ± 0.2 pF; $n = 70$) and a high input resistance (2.1 ± 0.3 GΩ; $n = 70$). In current-clamp mode at -60 mV (set by injecting currents of -10 to -20 pA), the ability of S-CSF-cNs to generate action potentials (APs) demonstrated their neuronal nature (Fig. 2*B*). The analysis of the AP discharge pattern indicated that S-CSF-cNs consisted of two neuronal populations: *tonic neurones* generating a train of APs (41%) and *phasic neurones* generating a single AP (59%) upon positive current injection (Fig. 2*B*; potassium chloride (KCl) solution with symmetrical chloride conditions, Table 1). However, when tested using a Mann–Whitney test, these two groups of neurones did not present any differences in their passive properties, i.e. membrane resistance of 2.5 ± 0.8 GΩ *vs.* 2.0 ± 0.4 GΩ ($P = 0.587$), membrane capacitance of 4.1 ± 0.4 pF *vs.* 3.6 ± 0.3 pF ($P = 0.332$) and a membrane resting potential of -42 ± 2 mV (minimum value: -51 mV, maximum value: -40 mV) *vs.* -43 ± 2 mV (minimum value: -69 mV, maximum value: -40 mV) ($P = 0.816$) for tonic ($n = 16$) and phasic neurones ($n = 23$), respectively. Finally, at resting membrane potential, S-CSF-cNs

pressure application of perfusion medium supplemented with 500 mM sucrose (10 s, black bar) evoked at -80 mV (V_h) a burst of synaptic events. Middle, expanded portions selected from the current trace at the top showing characteristic inward synaptic currents. Bottom, this sucrose-induced synaptic activity was completely blocked in the presence of 10 μM strychnine added to 1 mM kynurenic acid and 10 μM gabazine. *C*, top, in the presence of 1 mM kynurenic acid and 1 μM strychnine, to block both glutamatergic and glycinergic transmission, a similar protocol to that in *B* (30 s sucrose application, black bar) evoked a burst of synaptic events as can be better visualised on the selected expanded trace (middle). The sucrose-induced synaptic activity was completely blocked in the presence of 10 μM gabazine added to 1 mM kynurenic acid and 1 μM strychnine (bottom). *D*, summary bar graphs of average GABA (filled bar; $n = 4$) and glycine (open bar; $n = 6$) current amplitude (left) and decay time constant (right). In each cell, the decay time constant was obtained from the fit of the average current trace using a monoexponential function. $^{**}P < 0.01$. *E*, representative average GABAergic (left) and glycinergic (right) synaptic currents with the superimposed fit of the current decay (grey line, with the decay time constant of the illustrated cell above the traces). Bottom, for a better comparison of the current decays, GABAergic (black line) and glycinergic (grey line) currents shown at the top were normalised to the current peak and superimposed.

exhibited depolarising events resembling post-synaptic potentials accompanied by or triggering AP discharge (Fig. 2*C*, top panel; KCl-based intracellular solution, Table 1). This suggests that S-CSF-cNs might receive synaptic inputs (see below Fig. 3). This assumption was confirmed by recordings in voltage-clamp mode, where S-CSF-cNs showed at −80 mV an inward current activity with a fast onset and an exponential recovery typical of spontaneous synaptic activity (Fig. 2*C*, bottom panel and *D*). A closer examination of the voltage-clamp recordings indicated that most of the observed spontaneous inward currents were in fact single-channel openings. On average the unitary currents amplitude was around 4 times smaller than the spontaneous synaptic currents when recorded at –80 mV with a high KCl-based intracellular solution (synaptic current amplitude: -44 ± 3 pA *vs.* unitary current amplitude: -12.0 ± 0.8 pA; $n = 7$ and 10 cells, respectively; Fig. 2*D* and see below). In the rest of our study, on the one hand, we characterised the nature of the ionotropic receptors expressed on medullar S-CSF-cNs and their involvement in a synaptic activity, and on the other hand we analysed the recorded single-channel activity and determined its properties.

S-CSF-cNs express functional ionotropic receptors

A previous study on rat spinal S-CSF-cNs has demonstrated the presence of GABA-induced currents mediated by $GABA_A$ receptor activation (Marichal *et al.* 2009). We therefore tested the functional expression of $GABA_A$ receptors in mice medullar S-CSF-cNs using pressure application of GABA (1 mM, 50 ms). At −80 mV, in voltage-clamp mode, pressure application of GABA induced, in all tested S-CSF-cNs, large and robust inward currents with a mean peak amplitude of -3.3 ± 0.5 nA (Fig. 3*A*, top left; $n = 7$; KCl-based symmetrical chloride conditions, Table 1). The current–voltage relationship of the recorded GABA currents, determined at holding potentials ranging from −80 to +60 mV (with 20 mV increments) indicated that the currents reversed at a membrane potential of -11 ± 7 mV ($n = 4$) close to the calculated equilibrium potential for chloride ions ($E_{Cl} = +2$ mV with a KCl-based intracellular solution, Table 1). Finally, GABA-mediated currents were blocked by 10 μM gabazine, a selective antagonist for $GABA_A$ receptors (Fig. 3*A*, top left; inhibition of $94 \pm 1\%$; $n = 3$).

In all tested S-CSF-cNs, we also observed inward currents with a mean peak amplitude of -174 ± 45 pA during glycine application (1 mM, 100 ms; $n = 7$; Fig. 3*A* bottom, left). The analysis of the current–voltage relationship for the glycine-mediated current (holding potentials ranging from −80 to +20 mV with 20 mV increments) revealed a reversal potential of -27 ± 3 mV close to E_{Cl} set at −34 mV (potassium gluconate-based solution, Table 1; $n = 5$) and consistent with glycine-mediated chloride currents, an assumption confirmed by the strong block of the glycine-mediated currents observed in the presence of 10 μM strychnine, a selective antagonist for glycine receptors (Fig. 3*A*, bottom left; inhibition of $86 \pm 4\%$; $n = 5$).

In rat spinal cord, Stoeckel *et al.* (2003) demonstrated the presence of P_2X purinergic subunits on S-CSF-cNs and Marichal *et al.* (2009) recorded fast ATP-mediated currents. We therefore tested on murine medullar S-CSF-cNs pressure application of ATP (100 μM, 1–5 s; $n = 3$), a P_2X purinergic receptors agonist. However, in contrast to the situation observed for spinal S-CSF-cNs, we did not observe any response (data not shown). To rule out the possibility for a rapid ATP hydrolysis in the slice that could explain the absence of response, we also tested 2-Me-S-ATP, a non-metabolisable ATP analogue. However, pressure application of 2-Me-S-ATP (100 μM, 1–5 s; $n = 3$) did not elicit any response either (data not shown). As a further control, since neurones of the dorsal motor nucleus of the vagus nerve (DMNX) are known to express functional purinergic receptors (Nabekura *et al.* 1995), we tested both ATP and 2-Me-S-ATP application onto this neuronal population present in the same slice and could elicit current responses (data not shown).

Taken together, the results presented above therefore demonstrate that murine medullar S-CSF-cNs express functional ionotropic receptors for GABA and glycine, but no apparent ionotropic purinergic receptors. We next examined if the identified functional ionotropic receptors were involved in the observed synaptic activity.

Synaptic inputs onto S-CSF-cNs are GABAergic and glycinergic

As mentioned above, under voltage-clamp recording conditions at −80 mV, S-CSF-cNs exhibited inward currents similar to spontaneous synaptic activity (Figs 2*D* and 3*A*, right). This spontaneous synaptic activity was observed with a low frequency of 0.5 ± 0.1 Hz ($n = 11$). At −80 mV these synaptic currents recorded with a KCl-based intracellular solution (E_{Cl} set at +2 mV; Table 1) had on average an amplitude of -44 ± 3 pA (minimum amplitude: −5 pA; maximum amplitude: −248 pA; $n = 7$ cells and 262 events), a rise time of 1.2 ± 0.1 ms and a decay time constant of 11.4 ± 2.1 ms. Further, the plot of the rise time against the amplitude of the synaptic currents showed little correlation ($r^2 = 0.48 \pm 0.03$ obtained from a linear regression; $n = 7$ cells) suggesting a little shaping of synaptic events by electrotonic filtering. Finally these synaptic currents would be of GABAergic nature since they persisted in the presence of kynurenic acid but were blocked when adding 10 μM gabazine to the aCSF. However, in a few cells, some rare synaptic currents could still be observed in the presence of kynurenic acid and gabazine. To characterise this rarely occurring

synaptic activity, we forced vesicular release using the classical hyperosmotic shock (see Methods). Indeed, in the presence of 1 mM kynurenic acid and 10 μM gabazine, a situation where both glutamatergic and GABAergic ionotropic receptors are blocked, a 10 s application of hyperosmotic aCSF elicited a burst of synaptic events that was abolished by 10 μM strychnine (Fig. 3*B*; $n = 6$). These glycinergic synaptic currents had an average peak amplitude of -27 ± 4 pA and, at room temperature, a mean decay time constant of 3.6 ± 0.7 ms (Fig. 3*D*; $n = 6$ cells and from 35 to 80 events per cell; caesium acetate (CsAc)-based intracellular solution, see Table 1). To be able to compare GABAergic synaptic events with the glycinergic ones, we elicited GABAergic synaptic events and analysed their properties in the same recording conditions and following a similar hyperosmotic shock as in Fig. 3*B* (see above). The GABAergic transmission was isolated using bath application of 1 μM strychnine in the presence of 1 mM kynurenic acid (Fig. 3*C*). Under these recording conditions, a short application of the hyperosmotic solution induced, in the four tested S-CSF-cNs, a burst of synaptic activity that was fully blocked once 10 μM gabazine was added to the perfusion medium (Fig. 3*C* bottom; $n = 4$; CsAc-based intracellular solution, Table 1). The induced GABA synaptic events had an average peak amplitude of -25 ± 2 pA similar to the one measured for induced synaptic glycinergic currents ($P = 0.392$ for GABA *vs.* glycine events, non-parametric Mann–Whitney test). However, the mean decay time constant of GABAergic synaptic currents was significantly slower than the one measured for glycinergic synaptic currents (Fig. 3*D*; 10.4 ± 0.5 ms for GABA events; $n = 4$ cells and between 60 and 150 events per cell; $P = 0.004$ for GABA *vs.* glycine events, Mann–Whitney test) as can be seen from the normalised superimposed current traces in Fig. 3*E*.

These results therefore indicate that the synaptic activity recorded in S-CSF-cNs was due to the activation of both $GABA_A$ and glycine synaptic receptors. Finally, it is important to note that in the presence of gabazine and strychnine alone (no kynurenic acid) no synaptic activity could be recorded in S-CSF-cNs either spontaneous or following hyperosmotic shock ($n = 4$; data not shown). These results therefore indicate that S-CSF-cNs exclusively receive inhibitory synaptic currents mediated by $GABA_A$ and glycine receptors.

Medullar S-CSF-cNs express functional PKD2L1-like channels

PKD2L1 channels have been mainly studied in heterologous expression systems and are characterised by a large conductance, a non-selective cationic nature and an activity modulated by changes in both extracellular pH and osmolarity (see Introduction). We undertook a set of experiments to determine whether the channel carrying the unitary current recorded in S-CSF-cNs (Fig. 2*D*) is PKD2L1 and therefore shares all its properties.

Under voltage-clamp recording conditions and in the whole-cell configuration, all recorded S-CSF-cNs exhibited a spontaneously occurring single-channel activity (Figs 2*D* and 4). This channel activity represented a hallmark of S-CSF-cNs, since it was never observed in any of the EGFP negative cells recorded close to the cc. In most cells, only one level of opening was observed. In these cells, single-channel activity was characterised, at −80 mV, by an inward unitary current with an average amplitude of -11.6 ± 0.4 pA and a mean open probability (NP_O) of 0.028 ± 0.004 (Fig. 4; caesium chloride (CsCl)-based intracellular solution, Table 1; $n = 28$). In 16 out of the 28 recorded cells, a second level of similar absolute amplitude could be clearly detected but with a low probability of occurrence ($NP_O = 0.005 \pm 0.001$, $n = 16$; Fig. 4*A* and *B*). However, these recordings were obtained in the whole-cell configuration, which can present limitations for the accuracy in amplitude and kinetics analysis. So far, our attempts to record channel activity in outside-out mode were unsuccessful, presumably because of the very low expression of functional channels at the plasma membrane.

In order to determine the nature of the ion(s) flowing through the channel and the channel conductance, we recorded unitary currents at various holding potentials and analysed their current–voltage relationship. Figure 4*C* illustrates representative current traces obtained at holding potentials ranging from −80 to +40 mV (20 mV increments; Fig. 4*C*, left). For each holding potential, the unitary current amplitude was measured (Fig. 4*C*, middle) and plotted against the holding potential to determine the current–voltage relationship (Fig. 4*C*, right). In this cell, the reversal potential for the unitary current and the single-channel conductance, determined from the linear fit of the experimental data points, were +6 mV and 169 pS, respectively (Fig. 4*C*, right). However, since under these recording conditions E_{Cl} was set at +2 mV (CsCl intracellular solution, Table 1), and it was not possible to distinguish currents carried by anions from those carried by cations because both anionic and non-selective cationic currents would reverse close to 0 mV. To resolve this issue, we designed a new set of experiments and recorded, in the same cell, unitary currents and GABA-mediated chloride currents (pressure application of 1 mM GABA, 50 ms; see above). Recordings were carried out at holding potentials ranging from –80 to −20 mV (with 20 mV increments; Fig. 4*D*, left). Note that for a better comparison of the current–voltage relationships, GABA-mediated and unitary currents were normalised to the peak current measured at −80 mV. From the experimental data points, we established the current–voltage relationship for the

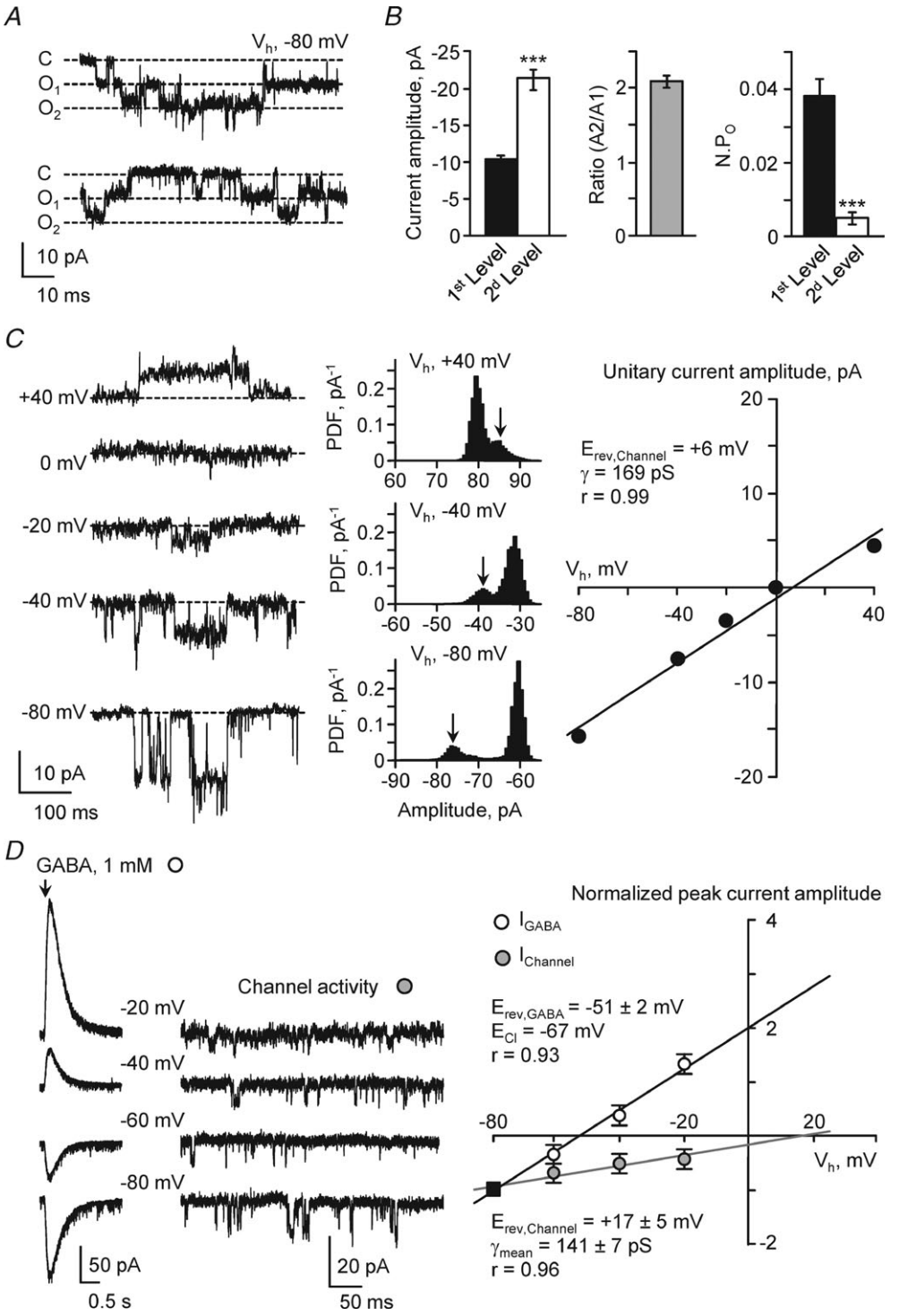

Figure 4. S-CSF-cNs present a spontaneous channel activity with properties similar to PKD2L1
A, current traces recorded at a holding potential of −80 mV (V_h) in one S-CSF-cN showing spontaneous single-channel activity. The dashed lines represent channel closed state (C, closed), first opening level (O_1) and second opening level (O_2), from top to bottom, respectively. *B*, left, summary bar graphs of the average current amplitude for the opening of one channel (1st level, filled bar; $n = 16$ cells) or two channels (2nd level, open bar; $n = 16$ cells). Middle, average ratio of the current amplitude measured from the second opening level (A_2) divided by the one measured at the first level (A_1). This ratio is close to 2 suggesting the simultaneous opening of two channels. Right, summary bar graph for the average channel open probability (NP_O) for the opening of one channel (1st level, filled bar; $n = 16$ cells) or two channels (2nd level, open bar; $n = 16$ cells). Note the very low occurrence of multiple opening events. ***$P < 0.001$. *C*, left, representative spontaneous single-channel current

unitary current and compared it, in the same cell, to that of GABA-induced currents (Fig. 4*D*, right). To be able to distinguish anionic currents (mostly carried by chloride ions) from the cationic ones, we set E_{Cl} at −67 mV using a CsAc-based intracellular solution (see Table 1). Here, the reversal potential, obtained from the experimental data, for $GABA_A$ currents ($E_{rev,GABA}$) was -51 ± 2 mV ($n = 6$ cells) tending towards E_{Cl}, as expected for $GABA_A$ currents, while the reversal potential for unitary currents remained more positive at $+17 \pm 5$ mV (Fig. 4*D*, right; $n = 6$ cells). The discrepancy between $E_{rev,GABA}$ and E_{Cl} (16 mV) might be due to the reported permeability of $GABA_A$ channels to bicarbonate that would shift $E_{rev,GABA}$ toward more positive values than E_{Cl} (Kaila *et al.* 1989). Due to uncompensated series resistance (10–20 MΩ), we cannot exclude an error in determining the membrane voltage that might also contribute to this discrepancy. However, this error may be small as we estimated a maximal error of 5–10 mV in the membrane voltage given maximal mean peak amplitude for the GABA-induced current of ±500 pA in this set of experiments. From the slope of the experimental linear current–voltage relationship for the unitary current, the conductance could be estimated to 141 ± 7 pS ($n = 6$ cells). Therefore, the spontaneously occurring unitary currents recorded in S-CSF-cNs shared two basic properties with PKD2L1 mediated currents: it was non-selective cationic and passed through an ionic channel of large conductance. To further support the identity between PKD2L1 channels and the channel activity recorded in S-CSF-cNs, we next determined how channel activity was modulated.

Single-channel activity is modulated by extracellular pH

In heterologous expression system, PKD2L1 activity was shown to be modulated by variation in extracellular pH (Ishimaru *et al.* 2006; Inada *et al.* 2008; Ishii *et al.* 2009; Shimizu *et al.* 2009). Therefore, we investigated in S-CSF-cNs the channel sensitivity to extracellular pH variation.

We first tested the effect of an extreme extracellular acidification on single channel activity. Pressure application for 10 s of a citric acid solution at pH 2.8 induced in all tested S-CSF-cNs (Fig. 5*A*), as well as in EGFP:PKD2L1 negative neurones (data not shown but see below Fig. 6), a biphasic response. This response was characterised by a fast inward and rapidly desensitising current (Fig. 5*A*; maximum: −190 pA, minimum: −126 pA and average peak amplitude of -170 ± 12 pA, $n = 9$; potassium gluconate-based intracellular solution, Table 1) followed by a sustained inward current of smaller amplitude that lasted for the whole duration of acid application. In agreement with the report of Shimizu *et al.* (2009), during this plateau phase, channel activity was fully blocked (Fig. 5*A*, bottom, Fig. 5*D* and Table 2; $n = 6$). Note that the plateau phase was not due to a sustained full activation of the unitary current but rather to the activation of a persistent acid sensing conductance (see below and Fig. 6*B*). The unitary current blockade mediated by citric acid at pH 2.8 was reversible and after a 20 s wash, NP_O returned to control values (Fig. 5*A*, bottom and *C*; wash: 0.023 ± 0.005 *vs.* control: 0.037 ± 0.014; $n = 6$, $P = 0.250$, Wilcoxon's test). This channel blockade was not due to citric acid itself but to extracellular acidification since a 30 mM citric acid solution buffered at pH 6.3 was without any effect on NP_O (Table 2; $n = 4$ and $P = 0.006$ *vs.* citric acid at pH 2.8, Mann–Whitney test). Moreover, the channel blockade was reproduced by application of a HCl solution at pH 2.8 (control: 0.025 ± 0.008 *vs.* HCl pH 2.8: 0.008 ± 0.004 and inhibition of 67 ± 16%; $n = 10$, $P = 0.008$, Wilcoxon's test and $P = 0.125$ *vs.* citric acid at pH 2.8, Mann–Whitney test). Because the effects of citric acid ($n = 6$) and HCl solutions ($n = 10$) at pH 2.8 were similar and not statistically different, we pooled the 16 cells responding to acidification. Under these conditions, the average NP_O was

traces recorded at holding potentials between −80 mV and +40 mV (in 20 mV increments) in one S-CSF-cN. Dashed line indicates channel closed state. Middle, representative all-points amplitude distribution histograms obtained from the recordings at holding potential of +40, −40 and −80 mV (from top to bottom). Arrow indicates for each holding potential the unitary current amplitude. Right, plot of the single-channel current amplitude against the holding potential obtained from the current traces illustrated on the left and calculated from the amplitude distribution histogram as illustrated in the middle. The unitary current reversal potential ($E_{rev,Channel}$) and the channel conductance (γ) were obtained from the linear fit of the experimental data points (black line). *D*, left, representative current traces recorded between −80 mV and −20 mV (20 mV increments) showing in the same S-CSF-cN the current response to GABA pressure application (1 mM, 50 ms, arrow) and the unitary current. Right, plot against the holding potential of the mean peak amplitude of the $GABA_A$ current (open circles, $n = 6$) and of the mean single-channel current amplitude (grey circles, $n = 6$) obtained from the current traces illustrated on the left. For a better comparison of the two current–potential relationships, in each cell the experimental data points were normalised against the current amplitude recorded at −80 mV (filled square). The reversal potential for $GABA_A$ current ($E_{rev,GABA}$) and for unitary current ($E_{rev,Channel}$) were obtained from the linear fit of the experimental data points. The values indicated on the graph correspond to the mean values ± SEM for $E_{rev,GABA}$, $E_{rev,Channel}$ and single-channel conductance (γ) obtained from the fit of the raw data recorded in 6 different S-CSF-cNs. Note that on average $E_{rev,GABA}$ tended towards E_{Cl} whereas $E_{rev,Channel}$ was more positive.

0.035 ± 0.006 in controls and was reduced by $77 \pm 11\%$ upon extracellular acidification.

In current-clamp recording mode, extracellular acidification with a citric acid solution at pH 2.8 induced an initial large depolarisation generating APs followed by a sustained smaller depolarisation lasting as long as acid application (Fig. 5*B*, top). These two phenomena represented a mirror image of the current recorded in voltage-clamp mode upon extracellular acidification (see top panels in Fig. 5*A* and *B*). Interestingly, at the end of acid application, an increased excitability with large depolarising events (several tens of millivolts) could be observed (Fig. 5*B*, bottom, voltage traces 4 and 5; $n = 3$).

Finally, it was proposed that cells expressing PKD2L1 may display a delayed rebound activity or 'off-response' once the acid stimulus was stopped (Ishimaru *et al.* 2006; Inada *et al.* 2008; Ishii *et al.* 2009; Kawaguchi *et al.* 2010). We therefore analysed the single-channel behaviour in the few seconds following the end of acid application to determine the presence of an 'off-response'. Indeed we could observe a single-channel rebound activity in S-CSF-cNs although in only 9 out of the 16 cells tested (Fig. 5*C*). In these 16 cells, unitary current activity was strongly reduced during the application of the extracellular pH 2.8 acid solution (citric acid and HCl at pH 2.8) and in 9 out of these 16 cells, once acidic application had

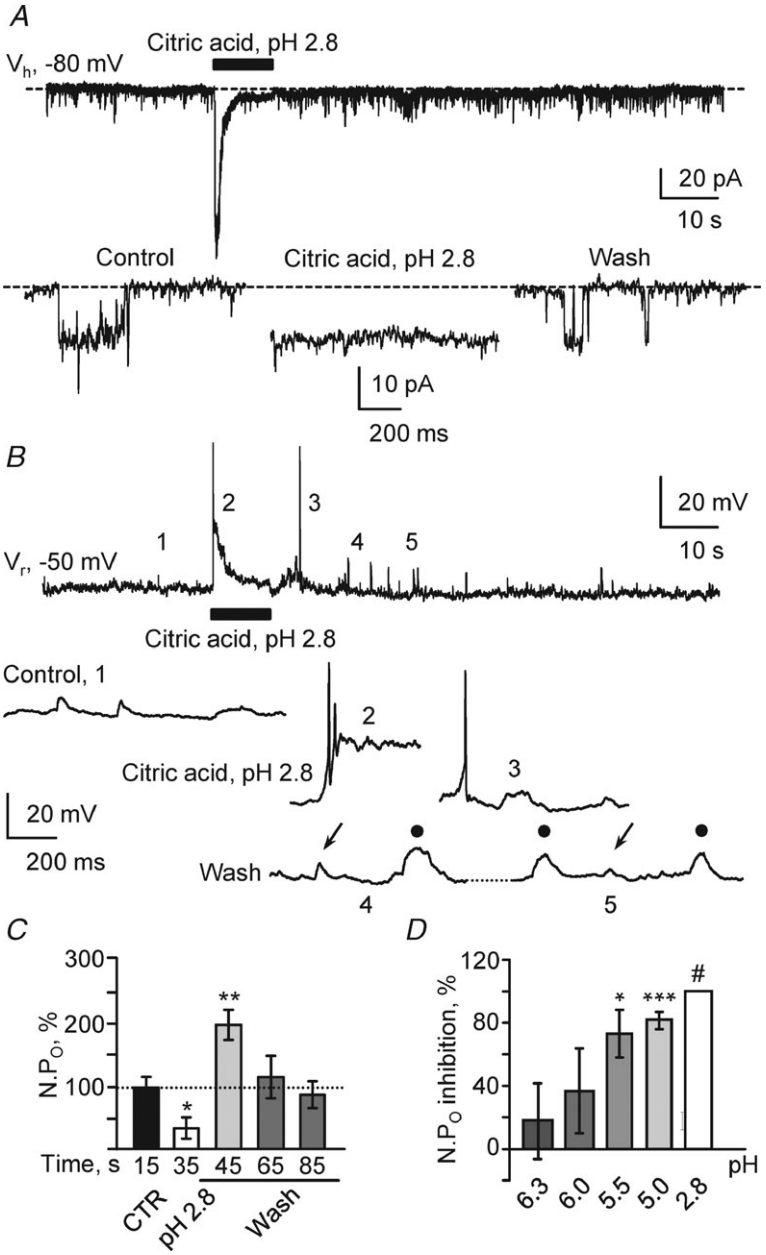

Figure 5. Acidification blocks unitary currents in a graded manner and modulates S-CSF-cNs excitability
A, representative spontaneous current trace recorded in voltage-clamp mode at −80 mV (V_h) in a S-CSF-cN before, during and after pressure application of a 30 mM citric acid solution at pH 2.8 (10 s; black bar). Bottom, expanded current traces selected from the recording at the top before (Control), during (Citric acid, pH 2.8) and after (Wash) extracellular acidification. Note the complete block of channel activity during extracellular acidification. Dashed line indicates channel closed state. *B*, representative voltage trace recorded in current-clamp mode at resting membrane potential ($V_r = -50$ mV) in the same S-CSF-cN as in *A* before, during and after extracellular acidification (Citric acid, pH 2.8, 10 s; black bar). Bottom, expanded voltage traces selected from the regions labelled with numbers on the voltage trace at the top before (Control; 1), during (Citric acid, pH 2.8; 2) and after (Wash; 3 to 5) extracellular acidification. Note that extracellular acidification evoked AP discharge at the start of citric acid application (2), presumably due to the inward current observed in voltage-clamp mode (see *A* top trace) and an increased depolarising activity at the end of exposure to acid (3). Interestingly on traces 4 and 5, depolarising events with kinetics similar to postsynaptic potentials (arrows) can be observed along with 'square-shaped' events (filled circles). *C*, summary bar graph for the variation in open probability (NP_O as a percentage) before (CTR, black bars), during (pH 2.8, open bars) and after (Wash, grey bars) pressure application of a pH 2.8 acid solution. Note the increased channel activity at the end of acidic exposure. NP_O values were obtained from recordings in 9 cells and represent mean values calculated over 10 s recording periods at the times indicated under the bars. *D*, summary histograms for the percentage of inhibition in NP_O following pressure application of citric acid solution with increased acidity: pH 6.3 ($n = 4$), pH 6.0 ($n = 5$), pH 5.5 ($n = 4$), pH 5.0 ($n = 5$) and pH 2.8 ($n = 6$). See also Table 2. For each pH condition, the NP_O during application was compared against the corresponding control NP_O and the percentage of inhibition calculated. $^{***}P < 0.001$; $^{**}P < 0.01$; $^{*}P < 0.05$, #full inhibition was observed for pH 2.8 and no statistical test could be performed.

stopped, the channel activity was increased by 100 ± 25% (Fig. 5*C*; with a rise in NP_O from 0.026 ± 0.004 in control to 0.052 ± 0.006 in the first 10 s of wash; $n = 9$; $P = 0.009$, Wilcoxon's test) without modification of the unitary current amplitude. Since the recordings were carried out using a CsCl-based solution it was not possible to correlate the presence of a single channel rebound activity with intrinsic firing properties (tonic *vs.* phasic AP discharge). Finally, to test for a graded inhibitory effect of extracellular acidification on single channel activity, we pressure applied different citric acid solutions with pH varying from 6.3 to 2.8. These results are summarised in Table 2 and in Fig. 5*D*. A significant reduction in NP_O was observed when pH was reduced below pH 5.5.

In neurones, exposure to acidic solution has been shown to induce activation of voltage-insensitive cationic channels of small conductance with a very high sensitivity to protons, the acid sensing ionic channels (ASICs; Waldmann *et al.* 1997; Deval *et al.* 2010). In response to extracellular acidification, ASIC activation elicits a fast inward rapidly desensitising current, which is, depending

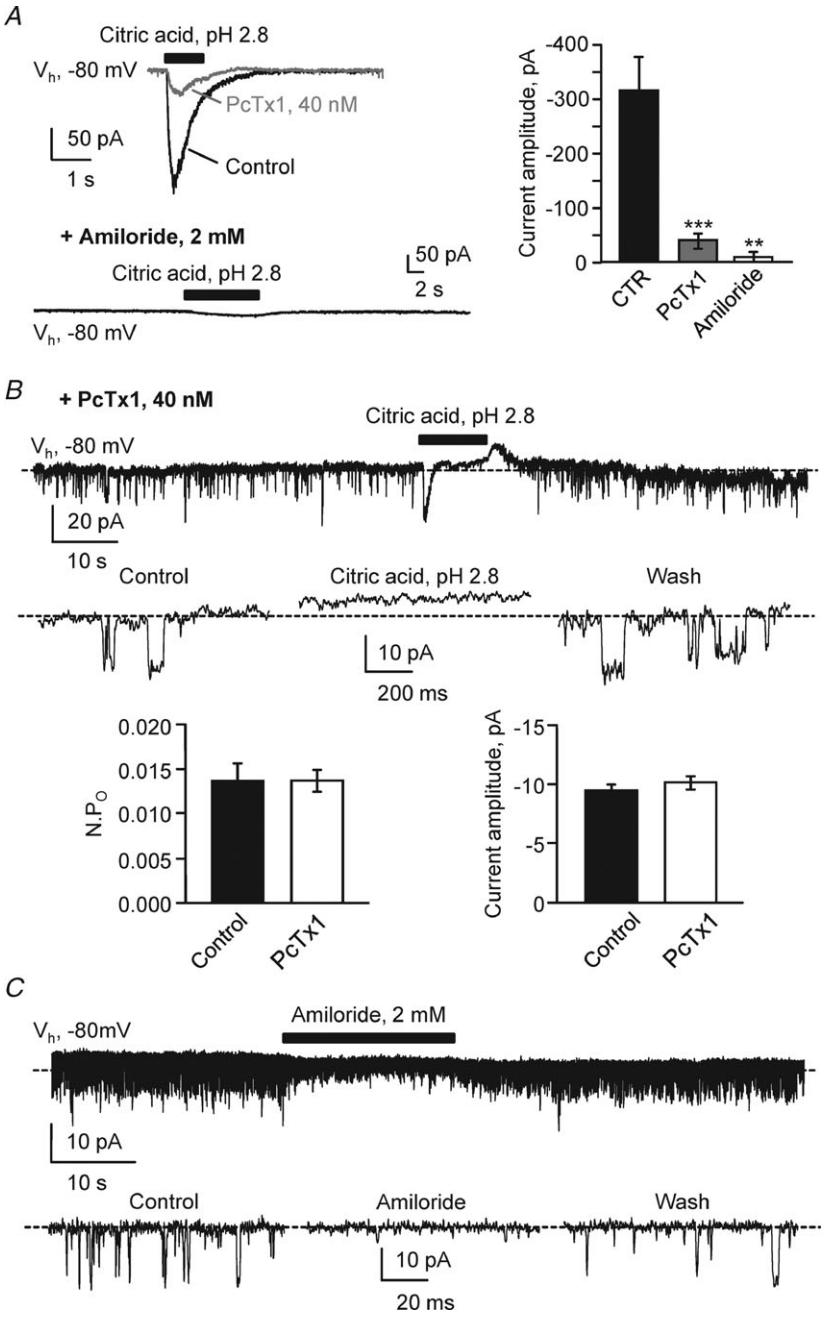

Figure 6. In CSF-CNs extracellular acidification elicits ASICs activation and subsequent inhibition of PKD2L1
A, left, typical current response recorded at −80 mV (V_h) in one S-CSF-cN following 1 s pressure application of a citric acid solution at pH 2.8 (1 s, black bar). Black and grey traces represent respectively recordings in control and in the presence of 40 nM PcTx1, a blocker of homomeric ASIC1a and heteromeric ASIC1a/2b. Bottom, in the continuous presence of 2 mM amiloride, the pH 2.8 citric acid-mediated current was blocked as well as single channel openings. Right, summary bar graph for the average acid-mediated current in control (black bar, $n = 14$), in the presence of 40 nM PcTx1 (grey bar, $n = 6$) and in the presence of 2 mM amiloride (open bar, $n = 4$). ***$P < 0.001$; **$P < 0.01$. *B*, top, representative spontaneous current trace recorded in a S-CSF-cN at −80 mV (V_h) in the presence of 40 nM PcTx1 before, during and after pressure application of a citric acid, pH 2.8 solution (10 s, black bar). Note that although the acid-mediated fast inward current is strongly reduced in the presence of PcTx1, an acid-sensitive channel activity can still be recorded. Middle, expanded current traces selected from the recording at the top before (Control), during (Citric acid, pH 2.8) and after (Wash) extracellular acidification. Dashed line indicates channel closed state. Bottom, summary bar graphs of the average NP_O (left) and unitary current amplitude (right) determined from 3 different cells before (Control, filled bars; $n = 3$) and in the presence of 40 nM PcTx1 (open bars, $n = 3$). *C*, representative current trace recorded at a holding potential of −80 mV (V_h) in one S-CSF-cN showing the reversible block of spontaneous channel activity following pressure application of 2 mM amiloride (20 s, black bar). Bottom, expanded current traces selected before (Control), during (Amiloride) and after (Wash) amiloride application from the recording at the top. Dashed line indicates channel closed state.

Table 2. Single-channel activity is increased by extracellular alkalinisation and inhibited by acidification in a graded manner

	TAPS		Citrate/citric acid based solutions									
Conditions	CTR	pH 8.8	CTR	pH 6.3	CTR	pH 6.0	CTR	pH 5.5	CTR	pH 5.0	CTR	pH 2.8
n	7		4		5		4		4		6	
Amp. (pA) ± SEM	−12.7 ± 0.7	−12.8 ± 0.7	−10.8 ± 0.3	−10.7 ± 0.6	−9.3 ± 0.8	−10.0 ± 1.2	−10.1 ± 0.6	−11.9 ± 2.4	−9.7 ± 0.4	−11.5 ± 1.3	−10.6 ± 0.9	–
P value #	0.672; NS		0.875; NS		0.765; NS		0.865; NS		0.665; NS		na	
NP_O ± SEM	0.025 ± 0.003	0.048 ± 0.006	0.037 ± 0.014	0.030 ± 0.009	0.012 ± 0.004	0.008 ± 0.003	0.016 ± 0.001	0.004 ± 0.002	0.023 ± 0.001	0.004 ± 0.001	0.037 ± 0.009	–
P value #	0.031*		0.062; NS		0.298; NS		0.022*		0.0001***		na	
NP_O variation	+88 ± 25%		−18 ± 23%		−37 ± 26%		−72 ± 14%		−82 ± 5%		Full inhibition	

Summary of mean unitary channel amplitude (Amp.), open probability (NP_O) and percentage of variation in NP_O following variation in extracellular pH compared to values measured in control situation (CTR). Extracellular alkalinisation: TAPS pH 8.8 ($n = 7$); extracellular acidification with citric acid solutions at pH between 6.3 and 2.8. A full inhibition was observed with citric acid solution at pH 2.8, therefore no statistical significance could be calculated for this condition. Except in the presence of citric acid pH 2.8, where unitary channel amplitude could not be measured, there was no change in the amplitude of the unitary current. $^*P < 0.05$; $^{***}P < 0.001$. CTR: control; TAPS: (*N*-tris(hydroxymethyl)methyl-3-aminopropanesulfonic acid. #Statistical test: Wilcoxon's matched-pairs signed rank test; NS: not statistically significant differences; na: not applicable.

on the subunit composition, accompanied or not by a sustained current of smaller amplitude (Deval *et al.* 2010). In order to test if the rapid inward current observed in S-CSF-cNs is carried by ASICs and more importantly exclude ASIC involvement in the spontaneously occurring single channel activity, we determined the sensitivity of the acid-mediated current to *Psalmopoeus cambridgei* toxin 1 (PcTx1), a selective blocker for homomeric ASIC1a and heteromeric ASIC1a/2b (Diochot *et al.* 2007; Baron *et al.* 2008; Sherwood *et al.* 2011).

As mentioned above (Fig. 5*A*), pressure application of a citric acid solution at pH 2.8 induced in all tested S-CSF-cNs, a fast inward and rapidly desensitising current (Fig. 6*A*). This current was reduced by 87% following bath application of 40 nM PcTx1 (Fig. 7*A* and *B*; maximum: −882 pA, minimum: −120 pA, average: −316 ± 55 pA in control, $n = 14$ *vs.* maximum: −74 pA, minimum: −16 pA, average: −40 ± 9 pA in PcTx1, $n = 6$; $P = 0.0006$, Wilcoxon's test). Note that PcTx1 application also blocked the sustained plateau current observed during prolonged acid exposure (Fig. 6*B*). This result therefore indicates that in S-CSF-cNs, ASICs are responsible for the biphasic current response (fast transient and plateau currents) observed following acid application. Further, although the acid-mediated inward current was largely blocked in the presence of 40 nM PcTx1, the toxin altered neither the NP_O (Fig. 6*B*, bottom left; 0.014 ± 0.006 in control *vs.* 0.014 ± 0.002 in PcTx1; $n = 3$, $P = 1.000$, Wilcoxon's test) nor the amplitude (Fig. 6*B*, bottom right; −9.5 ± 0.4 in control *vs.* −10.2 ± 0.4 in PcTx1; $n = 3$, $P = 0.182$, Wilcoxon's test) of the unitary current recorded in S-CSF-cNs. Moreover, during ASICs blockade with 40 nM PcTx1, acid application still suppressed single channel activity (Fig. 6*B*, top and middle). We also tested the effect of amiloride, a non-specific drug that blocks both ASICs (Holzer, 2009) and PKD2L1 channels (Ishimaru *et al.* 2006; Dai *et al.* 2007). As expected, when 2 mM amiloride was bath applied, no current response could be observed following short exposure to an acidic solution (Fig. 6*A*, bottom; −8 ± 3 pA in amiloride, $n = 4$; $P = 0.003$ *vs.* control, Wilcoxon's test) but also no single-channel activity was detected (Fig. 6*A*, bottom left). Note that, in the four S-CSF-cNs tested, the spontaneously occurring channel activity was reversibly blocked by pressure application of 2 mM amiloride alone (Fig. 6*C*). These results therefore indicate that S-CSF-cNs express functional ASICs responsible for the fast acid-induced current along with PKD2L1-like channels classically inhibited by acidic exposure.

In contrast, pressure application at −80 mV, in voltage-clamp mode, of a pH 8.8 TAPS-based solution reversibly increased the channel mean open probability by 88 ± 25% on average without affecting unitary current amplitude (Fig. 7*A* and Table 2; $n = 7$; potassium gluconate-based intracellular solution, Table 1). Note that in none of the experiments where extracellular pH was transiently modified was the single-channel amplitude affected (Table 2). The alkalinisation-mediated increase in single-channel activity was reversible, since 10 s after washing out the TAPS solution, NP_O returned to control value (Fig. 7*A*; wash: 0.035 ± 0.06 *vs.* control: 0.026 ± 0.004; $n = 7$ and $P = 0.310$, Wilcoxon's test). Finally, application of the TAPS solution at pH 8.8 induced APs discharge in the three S-CSF-cNs tested under current-clamp mode (Fig. 7*B*). One might therefore suggest that the higher single-channel activity induced by extracellular alkalinisation underlies the observed increased neuronal excitability.

Collectively, the results presented above first indicate that S-CSF-cNs express functional ASICs that are responsible for the initial fast current response following extracellular acidification and second show that extracellular acidification or alkalinisation decreased or increased single channel activity, respectively. These

results are additional arguments suggesting that PKD2L1 channels carry the unitary current recorded in medullar S-CSF-cNs.

Single-channel activity is modulated by variations in extracellular osmolarity

PKD2L1 channels have been proposed to act as mechano-receptors and to be modulated by variation in extracellular osmolarity, i.e. channel activity would be reduced or increased following an hyper- or hypo-osmotic challenge, respectively (Murakami *et al.* 2005; Shimizu *et al.* 2009). As a supplementary line of evidence for the functional expression of PKD2L1 in medullar S-CSF-cNs, we therefore determined the osmosensitivity of the unitary-current recorded in our model.

We first exposed S-CSF-cNs for 3 min to a hyperosmotic solution (Fig. 8*A*; from ∼310 to ∼355 mosmol kg^{-1}, see Methods). In all the cells tested, this hyperosmotic challenge affected neither the unitary current amplitude (-8.9 ± 0.3 pA in control *vs.* -9.0 ± 0.3 in hyper-osmotic condition; $n = 5$, $P = 0.733$, Wilcoxon's test; CsCl-based solution, Table 1) nor the NP_O (Fig. 8*A*; 0.012 ± 0.004 in control *vs.* 0.009 ± 0.002 in hyperosmotic condition; $n = 5$, $P = 0.291$, Wilcoxon's test). However, a 28% decrease in NP_O could be observed although not statistically significant (Fig. 8*A*, bottom right).

In contrast, under the same recording conditions, a 3 min exposure to a hypo-osmotic solution (from ∼310 to ∼265 mosmol kg^{-1}, see Methods) induced a strong increase in NP_O, i.e. $237 \pm 69\%$ in the three cells tested (Fig. 8*B*; 0.014 ± 0.003 in control *vs.* 0.046 ± 0.009 in hypo-osmotic condition; $n = 3$, $P = 0.009$, Wilcoxon's test) without affecting the unitary current amplitude (-9.3 ± 0.4 pA in control *vs.* -9.8 ± 0.4 in hypo-osmotic condition; $n = 3$, $P = 0.250$, Wilcoxon's test; CsCl based solution, Table 1). This increase in NP_O was reversible since, in all cells tested, NP_O returned to its control value following a 10 min wash (Fig. 8*B*, bottom right; 0.014 ± 0.003 in control *vs.* 0.014 ± 0.004 in hypo-osmotic condition; $n = 3$, $P = 0.820$, Wilcoxon's test). Therefore, the observed modulation of single-channel activity following hypo-osmotic shocks is a further argument pointing

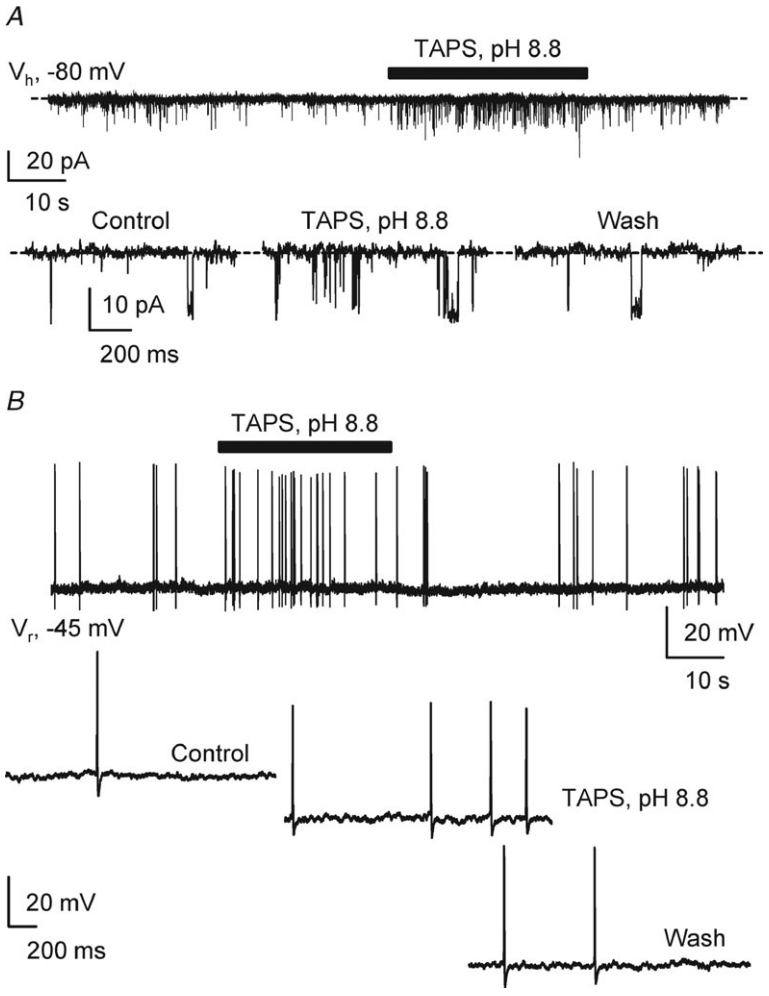

Figure 7. Alkalinisation increases both single-channel activity and excitability in S-CSF-cNs
A, representative spontaneous current activity recorded in voltage-clamp mode at −80 mV (V_h) in a S-CSF-cN before, during and after pressure application of a pH 8.8 TAPS-based alkaline solution (30 s, black bar). Bottom, expanded current traces selected from the recording at the top before (Control), during (TAPS, pH 8.8) and after (Wash) extracellular alkalinisation. Dashed line indicates channel closed state. Note the increased channel activity during extracellular alkalinisation (Middle). *B*, representative voltage trace recorded in current-clamp mode at resting membrane potential ($V_r = -45$ mV) in the same S-CSF-cN as in *A* before, during and after extracellular alkalinisation (TAPS, pH 8.8; 30 s, black bar). Bottom, expanded voltage traces selected from the trace shown at the top before (Control), during (TAPS, pH 8.8) and after (Wash) extracellular alkalinisation. Note that extracellular alkalinisation induces an increase in APs discharge (middle).

towards the functional expression of PKD2L1 channels in medullar S-CSF-cNs.

Discussion

Using PKD2L1:EGFP transgenic mice, we characterised for the first time the electrophysiological properties of medullar S-CSF-cNs. Here, we restricted our study to subependymal CSF-cNs with a soma close to the ependymal layer from which a neurite extended toward the cc and ended with a bud. Most studies aimed at characterising PKD2L1 channels and interfering with their properties have been conducted in cells that heterologously overexpressed PKD2L1 (Chen *et al.* 1999; Liu *et al.* 2002; Ishimaru *et al.* 2006; Ishii *et al.* 2009; Shimizu *et al.* 2009). PKD2L1 have been shown to be expressed by spinal S-CSF-cNs (Huang *et al.* 2006) and taste receptor cells in the tongue (Huang *et al.* 2006; Ishimaru *et al.* 2006; Kawaguchi *et al.* 2010). However, none of these studies have investigated PKD2L1 channel properties at the single channel level. This study represents the first recordings, in native neurones, of a PKD2L1-like unitary current and its modulation by extracellular pH and osmolarity.

CSF contacting neurones in mice brainstem

Although the presence of neurones in contact with the CSF had been demonstrated for decades in mammalian brain, most results are morphological and the exact distribution and function of CSF-cNs remain elusive (Vigh & Vigh-Teichmann, 1998; Vígh *et al.* 2004). To our knowledge, CSF-cNs have not been characterised in mice brainstem and only a few studies in vertebrate spinal cord have determined their morphological and electrophysiological properties (Stoeckel *et al.* 2003; Russo *et al.* 2004; Huang *et al.* 2006; Marichal *et al.* 2009; Reali *et al.* 2011). In these reports, subependymal CSF-cNs presented the same peculiar morphology as the medullar S-CSF-cNs described in the present study with a small soma projecting a single process toward the cc and ending with a spherical protrusion called bud (Stoeckel *et al.* 2003; Russo *et al.* 2004; Huang *et al.* 2006; Marichal *et al.* 2009; Reali *et al.* 2011). In our study, thin axon-like processes could be observed only over short distances, presumably because they run longitudinally (Vigh *et al.* 1977; Stoeckel *et al.* 2003) and were cut in our coronal slices. Further, a cilium extending from the bud of rat spinal S-CSF-cNs was reported using electron microscopy techniques (Stoeckel *et al.* 2003) or following cellular dialysis with a fluorescent

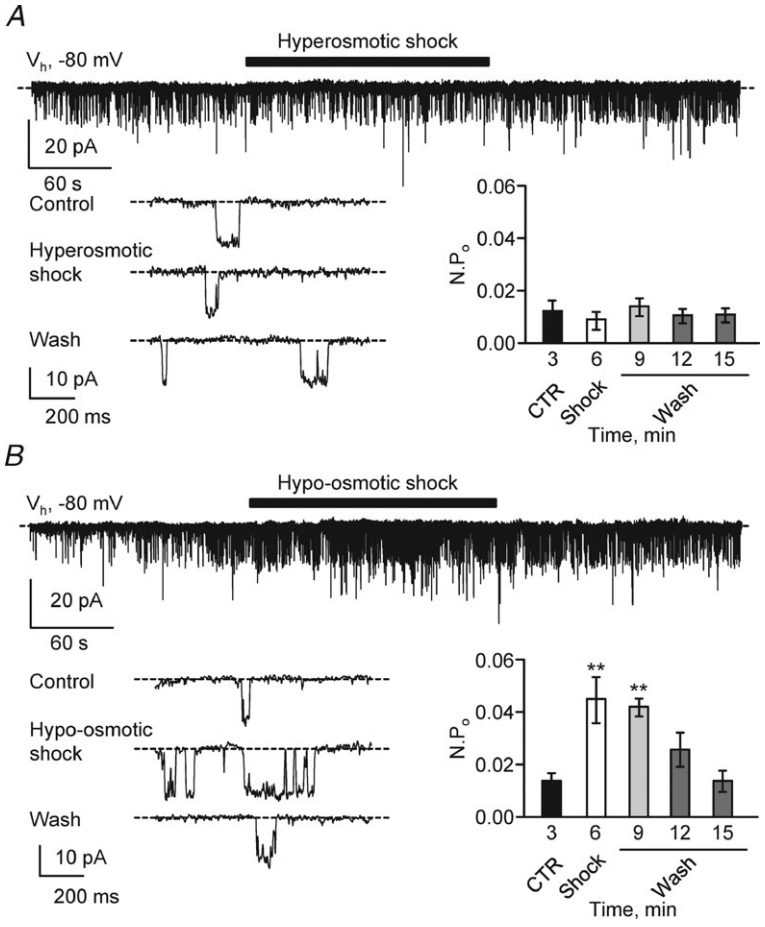

Figure 8. Extracellular hypo-osmotic shock strongly increases single-channel activity
A, top, representative spontaneous current trace recorded in a S-CSF-cN at −80 mV (V_h) before, during and after pressure application of a hyperosmotic solution (3 min; black bar). Bottom left, expanded current traces selected from the recording at the top before (Control), during (Hyperosmotic shock) and after (Wash) exposure to the hyperosmotic solution. Dashed line indicates channel closed state. Bottom right, summary bar graphs of the average NP_O determined before (CTR, black bar), during (Shock, open bar) and after (Wash, grey bars) pressure application of the hyperosmotic solution ($n = 5$ cells). *B*, top, representative spontaneous current traces recorded in a S-CSF-cN at −80 mV (V_h) before, during and after pressure application of a hypo-osmotic solution (3 min; black bar). Bottom left, expanded current traces selected from the recording at the top before (Control), during (Hypo-osmotic shock) and after (Wash) exposure to the hypo-osmotic solution. Dashed line indicates channel closed state. Bottom right, summary bar graphs of the average NP_O determined before (CTR, black bar), during (Shock, open bar) and after (Wash, grey bars) pressure application of the hypo-osmotic solution ($n = 3$ cells). In *A* and *B*, only the first 9 min of recordings are illustrated and in the histograms, NP_O represent mean values calculated over 3 min periods at the time indicated under the bars. $^{**}P < 0.01$.

marker (Marichal *et al.* 2009). We never visualised any structure resembling a cilium at the end of the bud in EGFP$^+$ or AlexaFluor 594 loaded medullar S-CSF-cNs. This discrepancy could either be due to technical issues where cilia would have been lost during the slicing procedure or to differences in morphology since CSF-cNs were suggested to represent a largely heterogeneous neuronal population (Vigh & Vigh-Teichmann, 1998; Vígh *et al.* 2004). Although we cannot rule out species or regional differences, this issue deserves to be addressed specifically in our model using appropriate histological techniques.

As mentioned above, mice medullar S-CSF-cNs shared numerous morphological properties with spinal S-CSF-cNs (Marichal *et al.* 2009). However, we demonstrated some strikingly different electrophysiological characteristics. First, in contrast with the three cellular types described by Marichal and colleagues (2009), we never observed S-CSF-cNs showing slow-depolarisation spikes indicative of an immature neuronal state. Most likely, the difference observed was due to the age difference between adult mice used in our study (P56–P70) and younger rats at different ages (neonatal, P0–P5 and juvenile, P15–P18). Second, we were unable to record the fast ATP-mediated currents elicited in rat spinal S-CSF-cNs (Marichal *et al.* 2009). As mentioned in Results, this might be due either to differences in species or to regional differences between spinal and medullar S-CSF-cNs. Finally, Marichal *et al.* (2009) mentioned the presence of events resembling postsynaptic potentials. Here, we demonstrated that medullar S-CSF-cNs exclusively receive GABAergic and/or glycinergic synaptic entries, and this result represents the first characterisation of functional inhibitory synaptic contacts onto this neuronal population. GABAergic neurotransmission is known to play an important role in the maturation of neuronal circuitry and switches from a depolarising action in the early developmental stages to a hyperpolarising one once the neuronal circuitry has matured (Ben-Ari, 2002). Such a dual action of GABA was recently demonstrated in spinal S-CSF-cNs and they were suggested to represent a population with neurones at various stages of maturity (Marichal *et al.* 2009; Reali *et al.* 2011). Therefore the physiological action of GABA and/or inhibitory transmission would need to be specifically addressed in mice medullar S-CSF-cNs to determine which physiological action $GABA_A$ receptors activation has on neuronal excitability and if medullar and spinal S-CSF-cNs share similar properties. Moreover, neither the exact origin of the fibres contacting medullar S-CSF-cNs nor the source of GABA is known. But numerous GABAergic neurones are interspersed in the solitary tract nucleus (Fong *et al.* 2005) and may be good candidates. On the other hand, spinal S-CSF-cNs were demonstrated to be GABAergic (Stoeckel *et al.* 2003) and may receive synapses from axon collaterals of neighbouring S-CSF-cNs as suggested by Vigh *et al.* (1977). We do not know if murine medullar S-CSF-cNs are GABAergic neurones and if such collaterals exist between medullar S-CSF-cNs. At this stage of the study, these two important questions remain open but will need to be specifically addressed in a dedicated study.

Single-channel activity in S-CSF-cNs and PKD2L1

All subependymal PKD2L1$^+$ CSF-cNs recorded in brainstem slices exhibited spontaneous single-channel activity that represented a hallmark for these neurones since this was never observed in EGFP negative cells even when localised close to the cc. Our data show that the unitary current recorded in S-CSF-cNs is due to the opening of a non-selective cationic channel of high conductance modulated by both extracellular pH and osmolarity (see above Figs 5, 7 and 8). Since all these properties have been reported for PKD2L1 channels overexpressed in oocytes and human embryonic kidney cells (HEK293T) (Chen *et al.* 1999; Ishimaru *et al.* 2006; Inada *et al.* 2008; Shimizu *et al.* 2009), one can assume that the single-channel activity recorded in S-CSF-cNs is carried by PKD2L1 channels.

Considering the strong immunoreactivity observed for PKD2L1 in S-CSF-cNs (see Fig. 1), it is surprising not to be able to record larger whole-cell PKD2L1-like currents. So far we were unsuccessful in recording PKD2L1 channels in the cell-attached or outside-out mode either from S-CSF-cNs somas or even from buds, which indicates an extremely low density of functional channels in the plasma membrane. In fact, in most cases, only one or two channels were recorded. This discrepancy could be explained by several mechanisms recently reported. Firstly, the functional stabilisation of PKD2L1 at the plasma membrane as well as the level of channel activity was suggested to depend on physical interactions between PKD2L1 and various partners. In the cases where such partners are absent or expressed at a lower level, PKD2L1 channel activity would be accordingly reduced (Murakami *et al.* 2005; Li *et al.* 2007; Inada *et al.* 2008; Ishimaru *et al.* 2010). Among these partners, PKD1L3, a polycystin subtype with 11 transmembrane domains, was shown to interact with PKD2L1 to enhance its activity, and to be involved in the 'off-response' observed following acid exposure (Murakami *et al.* 2005; Inada *et al.* 2008; Ishimaru *et al.* 2010). In medullar S-CSF-cNs we could record such an 'off-response' at the end of the acid exposure in more than half of the tested cells (see Fig. 5*C*). Moreover, preliminary results using RT-PCR techniques on tissues collected around the cc of the DVC indicated the presence of mRNA transcripts for both PKD2L1 and PKD1L3 (data not shown). Although PKD1L3 is not the only protein that may interact with PKD2L1, its presence in the brainstem makes it a good potential partner

capable of regulating channel activity as demonstrated in some taste cell receptors (Huang *et al.* 2006; LopezJimenez *et al.* 2006). On the other hand, Yang *et al.* (2012) recently demonstrated that receptor for activated C kinase 1 (RACK1), an anchoring protein, would interfere with membrane expression and activity of PKD2L1 channels. Secondly, PKD2L1, like PKD2, presents an endoplasmic reticulum (ER) retention signal that would lead to the preferential localisation of the channel at the ER membrane (Murakami *et al.* 2005; Li *et al.* 2007; Ishimaru *et al.* 2010). At this intracellular location they might play a role in the mobilisation of intracellular calcium from internal calcium stores since PKD2L1 channels are also permeable to calcium (Chen *et al.* 1999; Koulen *et al.* 2002). We do not know yet whether such a role in intracellular calcium homeostasis exists in S-CSF-cNs and if it could involve PKD2L1. Finally, PKD2L1 proteins have been localised in various cellular sites such as plasma membrane, ER and primary cilium, and trafficking between endoplasmic reticulum and plasma membrane does occur (Köttgen *et al.* 2005; Tsiokas *et al.* 2007). Such a regulated PKD2L1 trafficking from the ER and functional stabilisation in the plasma membrane could be another mechanism limiting PKD2L1 channel activity in medullar S-CSF-cNs.

Despite the low density of functional channels in the plasma membrane, our data also suggest that activation of a single PKD2L1-like channel is capable of modulating cell excitability. An increase in channel open probability by washout of acid solution (Fig. 5) or alkalinisation (Fig. 7) might lead to an enhanced AP discharge activity probably due to the high input resistance of S-CSF-cNs. Triggering action potentials by single channel opening has been previously observed in some high-resistive cells (Lynch & Barry, 1989; Johansson & Arhem, 1994). Therefore, one may suggest that, even at a low density, PKD2L1-like channels expressed at plasma membrane might play an important role in determining S-CSF-cN excitability. Thus it is important to investigate which cellular mechanisms control PKD2L1 channel activity and how they are regulated. Such a dedicated study would enable a better understanding of the function of the PKD2L1 channel especially in S-CSF-cNs.

Huang and colleagues (2006) as well as Marichal and colleagues (2009) showed that short extracellular acidification triggered an enhanced excitability in spinal S-CSF-cNs, and they both argue, although carefully, that it could involve PKD2L1 activity. We have a different interpretation. Our results show that S-CSF-cNs responded to a strong extracellular acidification (pH 2.8; Fig. 5*B*) by an ON and OFF burst of action potentials spaced by a plateau potential. The ON response consisting in a large inward desensitising current is most likely mediated by ASC1a containing channels because of its high sensitivity to psalmotoxin 1 (Baron *et al.* 2008). On the other hand, the PKDL21-like conductance is not involved in the ON response since we found that strong acidification totally inhibited the single channel activity as reported by others (Chen *et al.* 1999; Shimizu *et al.* 2009). Secondly, following the washout of the pH 2.8 acid solution, we recorded, in half of the tested cells, an increased single channel activity resembling the OFF response to acidification reported in HEK293T cells expressing PKD2L1 (Ishimaru *et al.* 2006; Inada *et al.* 2008) and in mouse taste cells (Kawaguchi *et al.* 2010). Interestingly, under current-clamp mode, we also observed following acid washout an increased excitability (Fig. 5*B*) that might be related to the observed enhanced PKD2L1-like channel activity. This suggests that extracellular acidification would be coded by both ASICs (ON response) and PKD2L1-like channels (OFF response). In contrast, as reported by Shimizu *et al.* (2009), we found that alkalinisation is more efficient to activate PKD2L1 channels. The variations in extracellular pH we used to test the modulation of the recorded unitary current are well beyond any pathophysiological pH value, even if one considers that large pH changes might occur locally. However, the choice for a pH 2.8 acid solution was motivated by protocols used in heterologous expression systems that enabled the characterisation of PKD2L1 properties, but we show that single channel activity was also significantly reduced by changes in extracellular pH around 5.5. It is worth noting that a pH sensitivity around pH 5.0 was also found in native taste cells from mouse circumvallate papillae (Kawaguchi *et al.* 2010). Overall, this sensitivity to extracellular pH points toward a chemosensitive function for S-CSF-cNs potentially carried by PKD2L1. At this stage, it is necessary to define under which physiological or pathological situation PKD2L1 might be activated and whether it confers a chemosensory role to S-CSF-cNs. Single channel activity was also modulated by change in extracellular osmolarity, especially following hypo-osmotic challenges, pointing to a possible mechanosensitive function for S-CSF-cNs namely a sensitivity to alteration of the cerebrospinal fluid balance or composition. Such chemo- and mechanosensitive functions remain to be proven, and the physiological contexts in which these medullar S-CSF-cNs might play a role in mammals remain to be found.

Concluding remarks

Little is known about the physiological role of CSF-cNs in the brain. At the level of the spinal cord, several studies proposed a function or involvement in neurogenic mechanisms and suggested that S-CSF-cNs represent a reservoir of immature neurones potentially activated following spinal injuries (Stoeckel *et al.* 2003; Marichal *et al.* 2009; Reali *et al.* 2011). Spinal S-CSF-cNs were also proposed to play a role in the control or induction of locomotion and swimming. Indeed in the zebra fish

larvae, the activation of spinal S-CSF-cNs, referred to as Kolmer Agdhur cells, would mimic spontaneous slow forward swimming (Wyart *et al.* 2009). It is unlikely that medullar S-CSF-cNs play a role in locomotion as the brainstem is a structure mainly involved in the regulation of autonomic functions (Guyenet, 2006; Schwartz, 2006 for review). In this context, a major field of research in our laboratory is studying the role of the DVC (see Fig. 1*A*) in energy homeostasis and particularly in the regulation of food intake. It is worth noting that the DVC integrates information of multiple origins: (i) neuronal from vagal and hypothalamic afferences, (ii) vascular via the area postrema, which is devoid of a blood–brain barrier, and (iii) circulating signals from the CSF. Many anorexigenic factors such as leptin, cholecystokinin, α-melanocyte stimulating hormone and orexigenic factors such as ghrelin and NPY are present in the CSF (Schwartz *et al.* 1996; Tritos *et al.* 2003; Popovic *et al.* 2004). The presence of CSF-cNs in DVC and hypothalamus, the two main brain structures regulating energy homeostasis, makes them good candidates for integrating CSF circulating signals known to affect food intake and homeostasis in general. This remains to be proven, which would require evaluating the sensitivity of CSF-cNs to these factors, and obviously identifying the targets of S-CSF-cNs, which remain so far totally obscure. Decoding the neuronal network that S-CSF-cNs are involved in represents the future challenge, essential for a better understanding of such a peculiar neuronal population conserved in the brain of all vertebrates.

References

Baron A, Voilley N, Lazdunski M & Lingueglia E (2008). Acid sensing ion channels in dorsal spinal cord neurons. *J Neurosci* **28**, 1498–1508.

Basora N, Nomura H, Berger UV, Stayner C, Guo L, Shen X & Zhou J (2002). Tissue and cellular localization of a novel polycystic kidney disease-like gene product, polycystin-L. *J Am Soc Nephrol* **13**, 293–301.

Ben-Ari Y (2002). Excitatory actions of gaba during development: the nature of the nurture. *Nat Rev Neurosci* **3**, 728–739.

Chen XZ, Vassilev PM, Basora N, Peng JB, Nomura H, Segal Y, Brown EM, Reeders ST, Hediger MA & Zhou J (1999). Polycystin-L is a calcium-regulated cation channel permeable to calcium ions. *Nature* **401**, 383–386.

Chuma T, Taguchi K, Kato M, Abe K, Utsunomiya I, Miyamoto K & Miyatake T (2002). Modulation of noradrenergic and serotonergic transmission by noxious stimuli and intrathecal morphine differs in the dorsal raphe nucleus of anesthtized rat: in vivo voltammetric studies. *Neurosci Res* **44**, 37–44.

Dai X-Q, Ramji A, Liu Y, Li Q, Karpinski E & Chen X-Z (2007). Inhibition of TRPP3 channel by amiloride and analogs. *Mol Pharmacol* **72**, 1576–1585.

Deval E, Gasull X, Noël J, Salinas M, Baron A, Diochot S & Lingueglia E (2010). Acid-sensing ion channels (ASICs): pharmacology and implication in pain. *Pharmacol Ther* **128**, 549–558.

Diochot S, Salinas M, Baron A, Escoubas P & Lazdunski M (2007). Peptides inhibitors of acid-sensing ion channels. *Toxicon* **49**, 271–284.

Fong AY, Stornetta RL, Foley CM & Potts JT (2005). Immunohistochemical localization of GAD67-expressing neurons and processes in the rat brainstem: subregional distribution in the nucleus tractus solitarius. *J Comp Neurol* **493**, 274–290.

Guyenet PG (2006). The sympathetic control of blood pressure. *Nat Rev Neurosci* **7**, 335–346.

Holzer P (2009). Acid-sensitive ion channels and receptors. *Handb Exp Pharmacol* 283–332.

Huang AL, Chen X, Hoon MA, Chandrashekar J, Guo W, Tränkner D, Ryba NJP & Zuker CS (2006). The cells and logic for mammalian sour taste detection. *Nature* **442**, 934–938.

Inada H, Kawabata F, Ishimaru Y, Fushiki T, Matsunami H & Tominaga M (2008). Off-response property of an acid-activated cation channel complex PKD1L3-PKD2L1. *EMBO Rep* **9**, 690–697.

Ishii S, Misaka T, Kishi M, Kaga T, Ishimaru Y & Abe K (2009). Acetic acid activates PKD1L3-PKD2L1 channel – a candidate sour taste receptor. *Biochem Biophys Res Commun* **385**, 346–350.

Ishimaru Y, Inada H, Kubota M, Zhuang H, Tominaga M & Matsunami H (2006). Transient receptor potential family members PKD1L3 and PKD2L1 form a candidate sour taste receptor. *Proc Natl Acad Sci U S A* **103**, 12569–12574.

Ishimaru Y, Katano Y, Yamamoto K, Akiba M, Misaka T, Roberts RW, Asakura T, Matsunami H & Abe K (2010). Interaction between PKD1L3 and PKD2L1 through their transmembrane domains is required for localization of PKD2L1 at taste pores in taste cells of circumvallate and foliate papillae. *FASEB J* **24**, 4058–4067.

Johansson S & Arhem P (1994). Single-channel currents trigger action potentials in small cultured hippocampal neurons. *Proc Natl Acad Sci U S A* **91**, 1761–1765.

Kaila K, Pasternack M, Saarikoski J & Voipio J (1989). Influence of GABA-gated bicarbonate conductance on potential, current and intracellular chloride in crayfish muscle fibres. *J Physiol* **416**, 161–181.

Kawaguchi H, Yamanaka A, Uchida K, Shibasaki K, Sokabe T, Maruyama Y, Yanagawa Y, Murakami S & Tominaga M (2010). Activation of polycystic kidney disease-2-like 1 (PKD2L1)-PKD1L3 complex by acid in mouse taste cells. *J Biol Chem* **285**, 17277–17281.

Köttgen M, Benzing T, Simmen T, Tauber R, Buchholz B, Feliciangeli S, Huber TB, Schermer B, Kramer-Zucker A, Höpker K, Simmen KC, Tschucke CC, Sandford R, Kim E, Thomas G & Walz G (2005). Trafficking of TRPP2 by PACS proteins represents a novel mechanism of ion channel regulation. *EMBO J* **24**, 705–716.

Koulen P, Cai Y, Geng L, Maeda Y, Nishimura S, Witzgall R, Ehrlich BE & Somlo S (2002). Polycystin-2 is an intracellular calcium release channel. *Nat Cell Biol* **4**, 191–197.

Li Q, Dai X-Q, Shen PY, Wu Y, Long W, Chen CX, Hussain Z, Wang S & Chen X-Z (2007). Direct binding of alpha-actinin enhances TRPP3 channel activity. *J Neurochem* **103**, 2391–2400.

Liu Y, Li Q, Tan M, Zhang Y-Y, Karpinski E, Zhou J & Chen X-Z (2002). Modulation of the human polycystin-L channel by voltage and divalent cations. *FEBS Lett* **525**, 71–76.

LopezJimenez ND, Cavenagh MM, Sainz E, Cruz-Ithier MA, Battey JF & Sullivan SL (2006). Two members of the TRPP family of ion channels, Pkd1l3 and Pkd2l1, are co-expressed in a subset of taste receptor cells. *J Neurochem* **98**, 68–77.

Lynch JW & Barry PH (1989). Action potentials initiated by single channels opening in a small neuron (rat olfactory receptor). *Biophys J* **55**, 755–768.

Marichal N, García G, Radmilovich M, Trujillo-Cenóz O & Russo RE (2009). Enigmatic central canal contacting cells: immature neurons in 'standby mode'? *J Neurosci* **29**, 10010–10024.

Meletis K, Barnabé-Heider F, Carlén M, Evergren E, Tomilin N, Shupliakov O & Frisén J (2008). Spinal cord injury reveals multilineage differentiation of ependymal cells. *PLoS Biol* **6**, e182.

Mothe AJ & Tator CH (2005). Proliferation, migration, and differentiation of endogenous ependymal region stem/progenitor cells following minimal spinal cord injury in the adult rat. *Neuroscience* **131**, 177–187.

Murakami M, Ohba T, Xu F, Shida S, Satoh E, Ono K, Miyoshi I, Watanabe H, Ito H & Iijima T (2005). Genomic organization and functional analysis of murine PKD2L1. *J Biol Chem* **280**, 5626–5635.

Nabekura J, Ueno S, Ogawa T & Akaike N (1995). Colocalization of ATP and nicotinic ACh receptors in the identified vagal preganglionic neurone of rat. *J Physiol* **489**, 519–527.

Nauli SM, Alenghat FJ, Luo Y, Williams E, Vassilev P, Li X, Elia AEH, Lu W, Brown EM, Quinn SJ, Ingber DE & Zhou J (2003). Polycystins 1 and 2 mediate mechanosensation in the primary cilium of kidney cells. *Nat Genet* **33**, 129–137.

Popovic V, Svetel M, Djurovic M, Petrovic S, Doknic M, Pekic S, Miljic D, Milic N, Glodic J, Dieguez C, Casanueva FF & Kostic V (2004). Circulating and cerebrospinal fluid ghrelin and leptin: potential role in altered body weight in Huntington's disease. *Eur J Endocrinol* **151**, 451–455.

Reali C, Fernández A, Radmilovich M, Trujillo-Cenóz O & Russo RE (2011). GABAergic signalling in a neurogenic niche of the turtle spinal cord. *J Physiol* **589**, 5633–5647.

Roux J, Wanaverbecq N, Jean A, Lebrun B & Trouslard J (2009). Depolarization-induced release of endocannabinoids by murine dorsal motor nucleus of the vagus nerve neurons differentially regulates inhibitory and excitatory neurotransmission. *Neuropharmacology* **56**, 1106–1115.

Russo RE, Fernández A, Reali C, Radmilovich M & Trujillo-Cenóz O (2004). Functional and molecular clues reveal precursor-like cells and immature neurones in the turtle spinal cord. *J Physiol* **560**, 831–838.

Sancesario G, Morello M, Massa R, Fusco FR, D'Angelo V & Bernardi G (1996). NADPH-diaphorase neurons contacting the cerebrospinal fluid in the ventricles of rat brain. *J Cereb Blood Flow Metab* **16**, 517–522.

Schwartz GJ (2006). Integrative capacity of the caudal brainstem in the control of food intake. *Philos Trans R Soc Lond B Biol Sci* **361**, 1275–1280.

Schwartz MW, Peskind E, Raskind M, Boyko EJ & Porte D Jr (1996). Cerebrospinal fluid leptin levels: relationship to plasma levels and to adiposity in humans. *Nat Med* **2**, 589–593.

Sherwood TW, Lee KG, Gormley MG & Askwith CC (2011). Heteromeric acid-sensing ion channels (ASICs) composed of ASIC2b and ASIC1a display novel channel properties and contribute to acidosis-induced neuronal death. *J Neurosci* **31**, 9723–9734.

Shimizu T, Janssens A, Voets T & Nilius B (2009). Regulation of the murine TRPP3 channel by voltage, pH, and changes in cell volume. *Pflugers Arch* **457**, 795–807.

Stoeckel M-E, Uhl-Bronner S, Hugel S, Veinante P, Klein M-J, Mutterer J, Freund-Mercier M-J & Schlichter R (2003). Cerebrospinal fluid-contacting neurons in the rat spinal cord, a gamma-aminobutyric acidergic system expressing the P2X2 subunit of purinergic receptors, PSA-NCAM, and GAP-43 immunoreactivities: light and electron microscopic study. *J Comp Neurol* **457**, 159–174.

Tritos NA, Kokkinos A, Lampadariou E, Alexiou E, Katsilambros N & Maratos-Flier E (2003). Cerebrospinal fluid ghrelin is negatively associated with body mass index. *J Clin Endocrinol Metab* **88**, 2943–2946.

Tsiokas L, Kim S & Ong E-C (2007). Cell biology of polycystin-2. *Cell Signal* **19**, 444–453.

Vígh B, Manzano e Silva MJ, Frank CL, Vincze C, Czirok SJ, Szabó A, Lukáts A & Szél A (2004). The system of cerebrospinal fluid-contacting neurons. Its supposed role in the nonsynaptic signal transmission of the brain. *Histol Histopathol* **19**, 607–628.

Vigh B & Vigh-Teichmann I (1998). Actual problems of the cerebrospinal fluid-contacting neurons. *Microsc Res Tech* **41**, 57–83.

Vigh B, Vigh-Teichmann I & Aros B (1977). Special dendritic and axonal endings formed by the cerebrospinal fluid contacting neurons of the spinal cord. *Cell Tissue Res* **183**, 541–552.

Waldmann R, Champigny G, Bassilana F, Heurteaux C & Lazdunski M (1997). A proton-gated cation channel involved in acid-sensing. *Nature* **386**, 173–177.

Wang QP & Nakai Y (1994). The dorsal raphe: an important nucleus in pain modulation. *Brain Res Bull* **34**, 575–585.

Wu G, Hayashi T, Park JH, Dixit M, Reynolds DM, Li L, Maeda Y, Cai Y, Coca-Prados M & Somlo S (1998). Identification of PKD2L, a human PKD2-related gene: tissue-specific expression and mapping to chromosome 10q25. *Genomics* **54**, 564–568.

Wyart C, Del Bene F, Warp E, Scott EK, Trauner D, Baier H & Isacoff EY (2009). Optogenetic dissection of a behavioural module in the vertebrate spinal cord. *Nature* **461**, 407–410.

Xiao M, Ding J, Wu L, Han Q, Wang H, Zuo G & Hu G (2005). The distribution of neural nitric oxide synthase-positive cerebrospinal fluid-contacting neurons in the third ventricular wall of male rats and coexistence with vasopressin or oxytocin. *Brain Res* **1038**, 150–162.

Yang J, Wang Q, Zheng W, Tuli J, Li Q, Wu Y, Hussein S, Dai X-Q, Shafiei S, Li X-G, Shen PY, Tu J-C & Chen X-Z (2012). Receptor for activated C kinase 1 (RACK1) inhibits function of transient receptor potential (TRP)-type channel Pkd2L1 through physical interaction. *J Biol Chem* **287**, 6551–6561.

Zhang L, Zeng Y-M, Ting J, Cao J & Wang M (2003). The distributions and signaling directions of the cerebrospinal fluid contacting neurons in the parenchyma of a rat brain. *Brain Res* **989**, 1–8.

Author contributions

The study was conducted in the Centre de Recherche en Neurobiologie-Neurophysiologie de Marseille (CRN2M), UMR 6231 CNRS-Universités Aix Marseille II et III – USC 2027 INRA, Département de Physiologie Neurovégétative and since the 1 January 2012 in the Laboratoire de Physiologie et Physiopathologie du Système Nerveux Somato-moteur et Neurovégétatif (PPSN) EA 4674 Aix-Marseille Université (AMU). A.O.: collection, analysis and interpretation of electrophysiological and immunohistochemical data; revising the manuscript critically for intellectual content. N.W.: conception and design of the experiments; collection, analysis and interpretation of electrophysiological data; analysis and interpretation of the immunohistochemical data; writing of the manuscript. C.T.: conception, design, collection, analysis and interpretation of the molecular biology experiments; revising the manuscript critically for intellectual content. V.T.: conception, analysis, interpretation of the immunohistochemical data and confocal imaging. M.D.: conception, collection, analysis and interpretation of the immunohistochemical data. J.T.: conception and design of the experiments; analysis and interpretation of data; writing of the manuscript.

Acknowledgements

We would like to thank Drs C. S. Zuker and P. Durbec for sending us transgenic mice models and Drs S. Diochot and E. Lingueglia for the generous gift the *Psalmopoeus cambridgei* toxin 1. We also acknowledge the University Paul Cézanne Microscopy Center (CP2M). This research was supported by funding obtained from University Paul Cézanne/Aix-Marseille III, the 'Région Provence-Alpes-Côte d'Azur', the 'Conseil Général des Bouches-du-Rhône' (PACA, CG13 – Neuracid, J.T.), and the PEPS 2010 from the CNRS INSB (Neuracil, N.W.).

Authors' previous address

Before the 1 January 2012 the authors have been at: Centre de Recherche en Neurobiologie-Neurophysiologie de Marseille (CRN2M), Département de Physiologie Neurovégétative, UMR 6231 CNRS-Universités Aix Marseille II et III USC 2027 INRA, France